Assessment of Some Atomization Models Used in Spray Calculations

M.S. Raju
ASRC Aerospace Corporation, Cleveland, Ohio

Dan Bulzan
Glenn Research Center, Cleveland, Ohio

NASA STI Program . . . in Profile

Since its founding, NASA has been dedicated to the advancement of aeronautics and space science. The NASA Scientific and Technical Information (STI) program plays a key part in helping NASA maintain this important role.

The NASA STI Program operates under the auspices of the Agency Chief Information Officer. It collects, organizes, provides for archiving, and disseminates NASA's STI. The NASA STI program provides access to the NASA Aeronautics and Space Database and its public interface, the NASA Technical Reports Server, thus providing one of the largest collections of aeronautical and space science STI in the world. Results are published in both non-NASA channels and by NASA in the NASA STI Report Series, which includes the following report types:

- TECHNICAL PUBLICATION. Reports of completed research or a major significant phase of research that present the results of NASA programs and include extensive data or theoretical analysis. Includes compilations of significant scientific and technical data and information deemed to be of continuing reference value. NASA counterpart of peer-reviewed formal professional papers but has less stringent limitations on manuscript length and extent of graphic presentations.

- TECHNICAL MEMORANDUM. Scientific and technical findings that are preliminary or of specialized interest, e.g., quick release reports, working papers, and bibliographies that contain minimal annotation. Does not contain extensive analysis.

- CONTRACTOR REPORT. Scientific and technical findings by NASA-sponsored contractors and grantees.

- CONFERENCE PUBLICATION. Collected papers from scientific and technical conferences, symposia, seminars, or other meetings sponsored or cosponsored by NASA.

- SPECIAL PUBLICATION. Scientific, technical, or historical information from NASA programs, projects, and missions, often concerned with subjects having substantial public interest.

- TECHNICAL TRANSLATION. English-language translations of foreign scientific and technical material pertinent to NASA's mission.

Specialized services also include creating custom thesauri, building customized databases, organizing and publishing research results.

For more information about the NASA STI program, see the following:

- Access the NASA STI program home page at *http://www.sti.nasa.gov*

- E-mail your question via the Internet to *help@sti.nasa.gov*

- Fax your question to the NASA STI Help Desk at 443–757–5803

- Telephone the NASA STI Help Desk at 443–757–5802

- Write to:
  NASA Center for AeroSpace Information (CASI)
  7115 Standard Drive
  Hanover, MD 21076–1320

Assessment of Some Atomization Models Used in Spray Calculations

M.S. Raju
ASRC Aerospace Corporation, Cleveland, Ohio

Dan Bulzan
Glenn Research Center, Cleveland, Ohio

National Aeronautics and
Space Administration

Glenn Research Center
Cleveland, Ohio 44135

March 2011

Acknowledgments

Level of Review: This material has been technically reviewed by technical management.

Available from

Assessment of Some Atomization Models
Used in Spray Calculations

M.S. Raju
ASRC Aerospace Corporation
Cleveland, Ohio 44135

Dan Bulzan
National Aeronautics and Space Administration
Glenn Research Center
Cleveland, Ohio 44135

ABSTRACT

The paper presents the results from a validation study undertaken as a part of the NASA's fundamental aeronautics initiative on high altitude emissions in order to assess the accuracy of several atomization models used in both non-superheat and superheat spray calculations. As a part of this investigation we have undertaken the validation based on four different cases to investigate the spray charactereristics of (1) a flashing jet generated by the sudden release of pressurized R134A from cylindrical nozzle, (2) a liquid jet atomizing in a subsonic cross flow, (3) a Parker-Hannifin pressure swirl atomizer, and (4) a single-element LDI (Lean Direct Injector) combustor experiment. These cases were chosen because of their importance in some aerospace applications. The validation is based on some 3D and axisymmetric calculations involving both reacting and non-reacting sprays. In general, the predicted results provide reasonable agreement for both mean droplet sizes (D_{32}) and average droplet velocities but mostly underestimate the droplets sizes in the inner radial region of a cylindrical jet.

NOMENCLATURE

B_k	Spalding mass transfer number
B_t	Spalding heat transfer number
C_p	specific heat, J/(kg K)
d	droplet diameter, m
dt	time increment, s
h	specific enthalpy, J/kg
k	thermal conductivity, J/(ms K)
l_k	mixture latent heat of evaporation, J/kg
$l_{k,eff}$	effective latent heat of evaporation, J/kg (defined in Eq. (6))
$\dot{m}$	liquid mass flow rate, kg/s
$\dot{m}_{k,flash}$	droplet vaporization rate under flash evaporating conditions, kg/s
$\dot{m}_{k,t}$	droplet vaporization rate due to heat transfer, kg/s
n_k	number of droplets in kth group
Nu	Nusselt number
P	pressure, N/m^2
Pr	Prandtl number
P_{sat}	saturation pressure, N/m^2
r_k	droplet radius, m
R_u	gas constant, J/(kg K)
Re	Reynolds number
Sh	Sherwood number
s_k	droplet radius-squared ($= r_k^2$), m^2
Sc	Schmidt number
SMD	Sauter mean diameter, m
t	time, s
T	temperature, K
T_b	boiling temperature, K
T_k	kth droplet temperature, K
U	gas or liquid velocity, m/s
x	axial distance, m
y	radial distance, m
Δp	pressure drop in the injector, N/m^2
μ	dynamic viscosity, kg/ms
ν	kinematic viscosity, m^2/s
ρ	density, kg/m^3
θ	spray cone angle, deg.

Subscripts

f	fuel
g	gas
inj	injector
l	liquid
r	radial coordinate

s	droplet surface
t	time
x	axial or x-coordinate
y	y-coordinate
z	z-coordinate

Superscripts

$^{-}$	mean, or average
$^{\cdot}$	flow rate

INTRODUCTION

Our previous work on spray modeling can be found in Refs. [1-10]. The spray solution procedure facilitates multi-dimensional spray/gaseous combustion calculations on massively parallel computers and unstructured grids. It also allows calculations to be performed in conjunction with the scalar Monte Carlo PDF (Probability Density Function) method [2]. The objective of our present investigation is two-fold:

(1) To develop a solution procedure based on the existing CFD models for the modeling of a superheated spray. An understanding of fuel atomization and vaporization behavior at superheat conditions is identified to be a topic of importance in the design of modern supersonic engines. The reasons for its occurrence are mainly two-fold [11-14]: it is because the same liquid fuel is often used as a coolant and the nozzles operate at low back pressures, and rapid depressurization across a fuel injection system may lead to flash injection because thermal inertia initially tends to maintain its internal liquid temperature above the saturation temperature when exit pressure falls into the superheated regime. Although flash evaporation is considered to be detrimental to engine performance under normal circumstances, it can have some potential benefits as it is known to produce a fine spray with enhanced atomization, increase effective spray cone angle, and decrease spray penetration [11].

(2) The success of any spray calculation depends a great deal on the specification of the appropriate injector exit conditions. In order to reduce uncertainty associated with the specification of the initial droplet conditions, we have undertaken a validation effort to establish accuracy of various atomization models used in spray calculations. They include the following models for primary atomization: (1) Blob-jet, (2) BLS (boundary layer stripping), and (3) Sheet-breakup, and the following models for secondary droplet breakup: (1) TAB (Taylor analogy breakup), and (2) ETAB (Enhanced Taylor analogy breakup). Further details of these models and their implementation can be found in [1].

In this paper, we first describe some details of the modeling approach used in the calculation of a superheated spray followed by a presentation of the results from our validation cases.

SUPERHEAT VAPORIZATION MODEL OF ZUO, GOMES, & RUTLAND [12], AND SCHMEHL & STEELANT [15-16]

A liquid is said to superheated when it is heated to a temperature above its boiling temperature. The atomization associated with a superheated spray is often referred to as flash atomization. The flashing phenomena refers to a process that is in thermodynamic non-equilibrium when a liquid is superheated [13-14]. We have adopted the modeling approach that was developed by Zuo, Gomes, and Rutland [12] and Schmehl and Steelant [15-16] for the vaporization model under superheat conditions. It is based on an extension of the classical D^2-theory. In the classical evaporation model, the thermal energy needed for evaporation is mostly furnished by the external heat transfer from the surrounding gas. Under superheat conditions, the characteristic vaporization time resulting from the external heat transfer from the surrounding gas is of the same order of magnitude as that resulting from the flash evaporation. The energy needed for vaporization at the droplet surface is partly provided by the superheat energy stored within the droplet but it is controlled by the droplet internal heat transfer. This modeling approach differs from the classical droplet vaporization models in three important ways: (1) the droplet surface mass fraction, Y_{fs}, approaches unity as the temperature at the droplet surface remains at the corresponding liquid boiling temperature under superheat conditions; (2) under superheat conditions, all the external heat transfer from the surrounding gas is made available to the vaporization process with no apparent increase in the droplet surface temperature; and (3) the flow of fuel vapor imparted by flash vaporization partly counterbalances the flow generated by external heat transfer which in turn may lead to a decrease in the energy transferred from the surrounding gas.

Based on the governing equations of conservation for an isolated spherically symmetric droplet, Zuo et al [12] and Schmehl and Steelant [15-16] showed that the total evaporation rate, $\dot{m}_k$, can be calculated as

$$\dot{m}_k = \dot{m}_{k,flash} + \dot{m}_{k,t} \qquad (1)$$

where the flash boiled vaporization rate, $\dot{m}_{k,flash}$, is given by

$$\dot{m}_{k,flash} = 4\pi r_k^2 \alpha_s \frac{(T_k - T_b)}{l_k} \qquad (2)$$

where T_k is the internal droplet temperature and the overall heat transfer coefficient, α_s $(= kJ/s\ m^2\ {}^oK)$ is given by the Adachi correlation [17]:

$$\alpha_s \begin{array}{ll} = 0.76(T_k - T_b)^{0.26} & (0 \le T_{ks} - T_b \le 5) \\ = 0.027(T_k - T_b)^{2.33} & (5 \le T_{ks} - T_b \le 25) \\ = 13.8(T_k - T_b)^{0.39} & (T_{ks} - T_b \ge 25) \end{array} \qquad (3)$$

which is valid over a wide range of superheat conditions. The vaporization rate due to external heat transfer, $\dot{m}_{k,t}$, in Eq. (1) is given by

$$\dot{m}_{k,t} = 2\pi r_k \frac{k}{C_p} \frac{Nu}{1 + \frac{\dot{m}_{k,flash}}{\dot{m}_{k,t}}} ln[1 + (1 + \frac{\dot{m}_{k,flash}}{\dot{m}_{k,t}})B_t] \qquad (4)$$

where the Spalding heat transfer number, B_t, is

$$B_t = \frac{C_p(T_g - T_{ks})}{l_{k,eff}} \qquad (5)$$

and the effective latent heat of vaporization, $l_{k,eff}$, is given by

$$l_{k,eff} = l_k + 4\pi \frac{\lambda_l r_k^2}{\dot{m}_k} \left(\frac{\partial T_k}{\partial r} \right)_s \qquad (6)$$

which is an useful parameter as it represents the total energy loss associated with the latent heat of vaporization in addition to the heat loss to the droplet interior. Finally, the Nusselt number, Nu, and the corresponding droplet regression rate, $\frac{ds_k}{dt}$, are given by

$$Nu = 2(1 + 0.3Re^{1/2}Pr_g^{1/3}) \qquad (7)$$

$$\frac{ds_k}{dt} = -\frac{\dot{m}_k}{2\pi r_k \rho_l} \qquad (8)$$

This model is valid over an entire range of superheat conditions as long as there is some amount of superheat energy available within the droplet $(T_k > T_b)$.

VAPORIZATION MODEL VALID UNDER NON-SUPERHEAT CONDITIONS

Under moderate superheat conditions, only a fraction of the vaporization takes place under superheat conditions $(T_k > T_b)$ and the remainder takes place under non-superheated evaporating conditions $(T_k \le T_b)$. So there is a need to revert back to a vaporization model valid under stable evaporating conditions when the internal droplet temperature approaches the boiling temperature. In the present calculations, the vaporization rate under normal evaporating conditions is evaluated by means of a simple classical D^2-theory:

$$\dot{m}_k = 2\pi r_k \rho_g\ D_{fgs}\ Sh\ ln(1 + B_k) \qquad (9)$$

where the Spalding mass transfer number, B_k, and the Sherwood number, Sh, are given by

$$B_k = \frac{(y_{fs} - y_f)}{(1 - y_{fs})} \qquad (10)$$

$$Sh = 2(1 + 0.3Re^{1/2}Sc_g^{1/3}) \qquad (11)$$

where y_{fs} is the mass fraction of the fuel species at the the droplet interface and y_f is the mass fraction of the fuel species in the surrounding gas.

INTERNAL DROPLET TEMPERATURE CALCULATION

Our experience with the validation studies showed us that there is a definite need to include a calculation involving the internal droplet temperature valid under both superheat and normal evaporating conditions. In our present calculations, it was evaluated by means of a simple infinite conductivity model.

$$\frac{dT_k}{dt} = -\frac{3[l_{k,eff} - l_k]}{2C_{pl}r_k^2} \frac{ds_k}{dt} \qquad (12)$$

$$if\ T_k \le T_b, \quad and$$

$$\frac{dT_k}{dt} = -\frac{3\alpha_s}{r_k \rho_l C_{pl}}(T_k - T_b) \qquad (13)$$

$$if\ T_k > T_b$$

SOME EFFECTS OF SUPERHEAT ON PRIMARY ATOMIZATION

Flash evaporation is known to produce a fine spray with enhanced atomization, increase effective spray cone angle, and decrease spray penetration [18]. Here, we consider the effects of flash evaporation on the primary atomization by following the approach of Zuo et al [12]. Its effect on the initial droplet size, d_{is}, is defined as a function of both engine pressure and a superheat parameter:

$$d_{is} = d_{in}(\frac{P}{P_{atm}})^{0.27}[1-\chi(\frac{P_{atm}}{P})^{0.135}] \quad 0 \le \chi(\frac{P_{atm}}{P})^{0.135} \le 1$$

(14)

where d_{in} is the corresponding droplet droplet size under normal evaporating conditions without flash evaporation, and χ, the superheat parameter, is defined as follows:

$$\chi = \frac{I(T_k) - I(T_b)}{l(T_b)}$$

(15)

where I is the internal energy of the liquid. Its value varies between $0 < \chi < 1$ with $\chi = 0$ referring to zero flash evaporation and $\chi = 1$ to full flash evaporation.

In Eq. (14), the increase in d_{is} due to an increase in engine pressure by a factor of $(\frac{P}{P_{atm}})^{0.27}$ is based on an experimental correlation obtained from Lefebvre [19]. It reflects the influence of chamber pressure on wave propagation as it damps wave growth. But the decrease by a factor of $(1 - \chi(\frac{P_{atm}}{P})^{0.135})$ is due to a significant reduction in droplet size caused by both cavitation and bubble growth under flash evaporation conditions. It was introduced based on the experimental observations from VanDerWege et al [20] and Reitz [21].

As the liquid approaches boiling, it also causes a substantial decrease in both intact liquid core length and core droplet size leading to a modification of the nominal cone angle, θ, as given by

$$\theta = \theta_n + (144 - \theta_n)\chi^2$$

(16)

where θ_n is in degrees for a spray vaporizing under normal conditions without flash evaporation. This correlation was developed based on the experimental data of Reitz [21]. These modifications from Zuo et al [12] were originally reported in conjunction with the sheet breakup primary atomization model but their validity with other primary atomization models needs further investigation.

RESULTS & DISCUSSION

A FLASHING JET GENERATED BY A CYLINDRICAL NOZZLE

We have spent considerable time on the literature survey in trying to identify some relevant experimental data for validation purposes. Of the limited data available, the recent experimental investigation by Yildiz et al [13-14,22] seems to be more promising as it contained data for two-phase jet flows associated with the near-field flashing phenomena generated by the sudden release of pressurized R134A from nozzles of different sizes with orifice-exit diameters ranging from 1, 2, and 4 mm. The experiments were performed mainly to simulate the effects of flashing phenomena generated by either of pressurized propane or butane. The reported data contained the particle image velocimetry (PIV) measurements of gas and droplet velocities, the phase Doppler anemometry (PDA) measurements of droplet sizes, the thermocouple measurements of temperatures, and the high speed images of flow visualization. While the data appeared to be worth pursuing, the reported experimental data contained a great deal of uncertainty with respect to the specification of the initial conditions. It is also noteworthy that the data had not gone through a rigorous review in terms of its applicability for validation purposes.

In the VKI experiments [13-14,22], the overall superheat conditions ranged between 40 to 50° C and the tank pressure ranged between 700 to 942 KPa [23]. For the conditions considered, the onset of jet breakup was observed to occur outside of the nozzle-exit between 2-27 mm for the 1mm nozzle, and 4-20 mm for the 2mm nozzle. But for the 4mm nozzle, a cloudy behavior was observed starting at 12mm with no discernible point of jet disintegration [23]. Our CFD calculations are focused primarily on predicting the flow characteristics further downstream beginning with the onset of jet breakup. At the start of jet dispersion, the pressurized liquid would undergo some expansion due to vaporization of the pressurized liquid depending on the degree of superheat and the entrainment of surrounding air [23]. Because of this expansion, the effective size of the expanded jet would be larger than the orifice exit [23]. Therefore, there is a need for estimating both the size and expansion angle of the jet from the observed experimental data [23].

In our present calculations, we have focused mainly on the case involving the 1mm nozzle for which the most extensive data were reported. For this case, the initial liquid temperature is 293 deg. K which corresponds to a superheat temperature of 46 deg. C. The initial liquid stagnation velocity is

estimated to be about 34 m/s based on the given up-stream and back pressures. Based on the data and the assumptions discussed in Ref. [23], the initial size of the jet at the point of jet breakup is estimated to be about 9mm. This is based on an initial estimated expansion angle of 55 to 60 deg. from X=1 to 3D.

All the calculations were performed on a 2D ax-isymmetric grid with 79101 triangular elements. The calculations were advanced until a steady state so-lution was reached by making use of the following time steps: Δt_g (= local time step used in the flow solver, s) was determined based on a CFL number of 1, $\Delta t_{injection}$ (time-step at which a new group of droplets is introduced) = 2.0 ms, and Δt_k (time step used in the spray solver) = 0.0075 ms. The initial gas conditions were prescribed based on the non-dimensional velocity profile reported in Ref. [14]. The initial droplet injection velocity and the initial liquid temperature are specified to be 34 m/s and 293 deg. K, respectively.

In this paper, we present the results obtained from two sets of calculations. Both the calculations are based the blob-jet model for primary atomization and the ETAB model for secondary droplet breakup. In Calculation 1, no effect of flash-induced atomiza-tion is taken into account. In Calculation 2, the ef-fects of flash-induced atomization are taken into ac-count as described earlier.

First, we would like to show the observed and predicted spray patterns. Fig. 1 shows an experimen-tal photograph obtained by means of a high-speed photography for the two-phase flashing jet generated by a 1mm nozzle (taken from Yildiz et al [22]). The corresponding axisymmetric spray pattern as pre-dicted by our CFD computations from Calculation 1 is shown in Fig. 2. It is also noteworthy that there is no direct correspondence in the scales used between the experiments and predictions. The results from Calculation 2 are also similar to Calculation 1.

1. Gas Velocity Comparisons

Shown in Figs. 3a & 3b are the gas veloc-ity comparisons with the experimental data. In the radial profiles of gas velocity, the velocity is non-dimensionalized by means of U/U_{max} and the radial distance by $r/D/(r/D)_{U_{max}/2}$.

The measurements were taken at three axial lo-cations, x/D = 110, 220 , and 440, The normalized experimental data represent the combined data re-ported over all three axial locations. It is noteworthy that the reported gas velocities were actually based

on the measured velocities of droplets of sizes smaller than ten microns. The non-dimensional velocity pro-files from the experimental data were shown to ex-hibit a self-similar behavior as given by the following correlation [14]:

$$\frac{U}{U_{max}} = exp[-0.693(\frac{r}{\bar{r}})^2] \qquad (17)$$

where $\bar{r} = r(U_{max}/2)$. This behavior was noted to be similar to other correlations reported in the literature [24-26] on both single and two-phase turbulent jets.

The velocity comparisons from Calculation 1 are shown in Fig. 3a, and those from Calculation 2 are shown in Fig. 3b. Also shown in Figs. 3a & 3b are the profiles as obtained from Eq. (17). The pre-dicted results are shown separately for each one of the three axial locations, x/D = 110, 220 , and 440. In both the calculations, the predicted gas velocities fall entirely within the scatter range of the experimental data. However, outside the experimental range, the CFD results at the first two axial locations overpre-dict the gas velocity as given by Eq. (17).

2. Droplet Velocity Comparisons

Shown in Figs. 4a-c & 5a-c are the non-dimensional droplet velocity profiles from Calcula-tions 1 & 2, respectively. Once again the velocity is non-dimensionalized by U/U_{max}, and the radial dis-tance by $r/D/(r/D)_{U_{max}/2}$. According to Yildiz et al [14], the non-dimensional droplet velocity profiles also followed a self-similar behavior as given by Eq. (17). The experimental data was based on the PDA measurements of all droplets with sizes higher than 10 μm. Again, the normalized experimental data rep-resent the combined data taken over all three axial locations. It is not entirely evident as to why the ve-locities for both gas phase and the droplets follow the same correlation.

Some noteworthy aspects of the comparisons from Figs. 4a-c & 5a-c are: (1) The CFD results show a general trend similar to the experimental data but exhibit a wider scatter than the experiments. (2) In both the calculations at x/D = 110, most of the predicted velocities are found to be located in the up-per range of the experimental data. It is because of the way we specified the initial conditions where the initial velocities for all droplets were assumed to be the same as the injection velocity of the liquid jet, 34 m/s. However, the predicted velocity range improves considerably further downstream at the the last two

axial locations. (3) The scatter in the predicted velocities seem to widen with the increased axial distance. (4) The results from Calculation 1 are in slightly better agreement as more of its predicted velocities fall within the experimental range.

3. Droplet Size Comparisons

Shown in Figs. 6a-c & 7a-c are the comparisons between the average droplet sizes (local SMD, D_{32}) versus the non-dimensional radial distance, r/D. Figs. 6a-c provide the comparisons from Calculation 1 at the three axial locations, x/D = 110, 220 , and 440. Similar comparisons from Calculation 2 are shown in Figs. 7a-c.

As can be seen from the experimental data in Figs. 6a-c & 7a-c, the experimental data exhibit a general trend that is typical of a cylindrical liquid jet where the larger droplets tend to be located near the centerline [14]. Away from the centerline, the experimental data show that there is a slight increase in the overall droplet size distribution with an increase in the axial distance. This effect is more evident in the comparisons between the last two axial locations. The reasons for this behavior can be attributed to the faster evaporation of smaller droplets which leaves the remaining size distribution with relatively large-size droplets [14].

Some highlights of the predictions from Calculation 1 (Figs. 6a-c) are as follows: (a) The experimental data show a much wider radial variation in the droplet sizes when compared with the predictions but the predictions manage to calculate the overall SMD with a reasonable accuracy. (b) At the first axial location, x/d =110, the droplet sizes are predicted with reasonable accuracy but at the last two axial locations, x/d = 220 & 440, they fall short of experimental data in the central region of the spray. The reasons for this behavior could be attributed for not taking into consideration the effect of droplet coalescence. It was reported to play a major role in the central region of a non-superheated spray [27]. Unfortunately, we can't verify this for a fact as we don't have a droplet coalescence model in our present code. (c) Away from the central region, the predicted sizes are in reasonable agreement with the experimental behavior.

The results from Calculation 2 (Figs. 7a-c) are similar to those obtained from Calculation 1. But the results from Calculation 2 underpredict the droplet sizes even more those from Calculation 1 in the central region of the spray at x/D = 110 & 220. This reduction in the droplet sizes could be primarily attributed to the superheat correction as introduced by Eq. (14). This correction leads to a reduction in the initial blob size during the primary atomization regime to about 500 μm from 1000 μm (=the injector diameter of the cylindrical nozzle).

4. Temperature Comparisons

The reported temperature data of Ref. [22] is based on the hot-wire thermocouple measurements which can't be used for making any direct comparisons with either predicted gas or liquid temperatures. To understand the reasons behind it, we provide some details on the nature of the temperature measurements obtained by Ref. [22]. The steady-state temperature measurements were obtained by means of a thermocouple made up of Chrome/Alumel wire of 0.2mm diameter represents an aggregate (liquid-gas) temperature. Therefore, its usefulness in making direct comparisons with either gas or liquid temperatures obtained from the CFD calculations becomes difficult. This consideration becomes more evident when we look at Fig. 8 which shows the single-point thermocouple temperature signal versus time (taken from Ref. [22]). Initially, the thermocouple registers a temperature of 293 deg. K (= ambient gas temperature) before it reaches a steady-state temperature of 248.7 deg. K ($\approx$ the boiling temperature of R134A). Also, because of the intrusive nature of the technique (taken by a thermocouple rack), the reported temperatures represent an aggregate temperature in the neighborhood of the centerline.

Figs. 9a-b show the axial variation (centerline) of the measured temperatures as well as the predicted gas and liquid temperatures from Calculations 1 & 2. The liquid temperatures represent the mass-averaged droplet temperatures. The results are similar from both the calculations. Initially the predicted gas temperatures are close to an ambient temperature of about 296° K before falling off to a level close to the measured temperature of about 225° K near x/D = 20. Further downstream, the predicted gas temperatures raise above the measured temperatures due to the entrainment of some surrounding gas from the ambient. On the other hand, the average droplet temperatures overpredict the measured temperatures initially before falling below the experimental data further downstream. It is also noteworthy that the experimental data show that a considerable amount of vaporization takes place under non-superheated conditions where the measured temperatures are lower

than the boiling temperature of R134A (=247 ^{o} K).

A LIQUID JET ATOMIZED IN A SUBSONIC CROSS-FLOW

This case was undertaken mainly to test the following models: BLS or blob-jet for primary atomization & ETAB for secondary droplet breakup. The experimental data for this validation case was taken from Ref. [28]. It involves the modeling of a liquid jet atomizing in a subsonic cross-flow based on a 3D calculation (non-reacting & turbulent air-flow). In this experiment, a liquid jet is injected vertically upward into a subsonic wind tunnel with the nozzle exit flush with the bottom wall [28]. The tunnel has a width of 125 mm, a height of 75 mm, and a length of 406 mm. The nozzle exit diameter is 0.5 mm. The reported measurements include droplet size, axial velocity, and volume flux at three x/D (=200, 300, & 500) locations. The test conditions for the case studied are as follows: The water is used as a test liquid with a liquid density of 998 kg/m^2, viscosity 0.000956 kg/m/s, and surface tension 0.0705 N/m. The liquid mass flow rate is about 0.0025 kg/s and a corresponding initial liquid velocity of 19.3 m/s. The cone spray angle is specified to be 10 degrees. For the gas phase at the inlet: the reference pressure is 140,000 Pa, the ambient temperature is 298 K, the air density is 1.633 kg/m^3, & the Mach number is 0.2 which corresponds to an axial velocity of 103.8 m/s (v=w=0.0).

We have performed two different calculations for this case: the first with the blob-jet primary atomization model and the second with the BLS primary atomization model. Both the calculations make use of the ETAB secondary droplet breakup model and the standard k-epsilon model for gas turbulence. They were performed on a grid with a mesh size of 34560. The grid for this case was provided by CFDRC. Fig. 10 shows the 3D perspective view of the axial gas velocity contours together with a spray pattern from Calculation 1. In this figure, the inlet boundary is located at $x = 0$, the exit boundary at $x = 0.3$, the bottom and top walls are located at y = 0 & 0.08, respectively, & the symmetric boundary conditions are applied at z = -0.05 and 0.05. The air flow is from the back to the front and the inflow air velocity is maintained at about 104 m/s. The velocity contours indicate that there is a little change in the overall gas velocity from 104 m/s other than a slight fall-off downstream of the nozzle exit in the region between the bottom wall and the spray. The spray is injected from the middle of the bottom wall at x = 0.05. The

spray is deflected towards the gas flow soon after its injection from the bottom wall. The outward spreading of the spray is also evident from the time of its inception near the nozzle location before it exits out of the computational domain.

Fig. 11 shows the droplet velocity comparisons at x/D = 200. The comparisons include the experimental data, and the results from both BLS and blob-jet primary atomization models. The results for the axial, radial and tangential velocities are shown in separate figures. Unfortunately, there is no reported experimental data for the radial and tangential velocities. The experimental data for the axial velocities are mostly in reasonable agreement with the predictions obtained from both blob-jet and BLS models. While it is true that the results mostly underpredict the experimental data, the comparisons show slightly better agreement with the results obtained from the blob-jet model. The BLS model mostly overpredicts the radial velocities from the blob-jet model by a small measure. The tangential velocities from both the models fall within the scatter range of each other but the results from the blob-jet model show a much wider scatter range. Similar comparisons are found in Fig. 12 at x/D = 300.

Fig. 13 shows the droplet size (D_{32}) comparisons at x/D = 200. The comparisons include the experimental data, and the results from both the BLS and blob-jet primary atomization models. The results from the blob-jet model are in better agreement but mostly underpredict the experimental data. Similar comparisons are found in Fig. 14 at x/D = 300.

PARKER-HANNIFIN PRESSURE SWIRL ATOMIZER

This case is undertaken mainly to test the following models: the sheet-breakup model for primary atomization, & the ETAB model for secondary droplet breakup. The experimental data for this case was reported by Ref [29]. It involves the modeling of a liquid spray generated by a pressure swirl atomizer based on an axisymmetric calculation (non-reacting & turbulent air-flow). In this experiment, the injector is located in the middle of a centerbody configuration, it has an exit diameter of 0.0012 m, and the internal pressure drop across the injector is 344500 Pa. The liquid mass flow rate is 0.00125 kg/s, the liquid fuel is $C_{12}H_{23}$, and the initial liquid temperature is 300 deg. K. It produces a hollow cone spray with a full-cone angle of 82 deg. & a half-cone angle of 15 deg.

The calculations for this case were performed on a 2D axisymmetric grid with 10201 triangular elements. The grid for this case was again provided by CFDRC. The calculations are advanced until a steady state solution was reached by making use of the following time steps: Δt_g (= local time step used in the flow solver, s) was determined based on a CFL number of 1, $\Delta t_{injection}$ (time-step at which a new group of droplets is introduced) = 1.0 ms, and Δt_k (time step used in the spray solver) = 0.01 ms. Along the left boundary of the 2D grid, a split boundary condition is implemented: a wall boundary condition is applied over the centerbody region from y = 0.0 to 0.019 m, and a inflow boundary is applied over y = 0.019 to 0.3 m. At the inflow boundary, the axial gas velocity (u) is assumed to be uniform at 1.2 m/s, the initial gas temperature is 300 deg. K, and the initial radial velocity profile is prescribed based on a linear interpolation: at y = 0.019 m, v = -0.9m/s, at y = 0.1 m, v = -0.5 m/s, & at y = 0.3 m, v=0. The lower boundary of the 2D grid is determined based on a symmetric boundary condition, and the exit boundary conditions are implemented at both the upper and left boundaries.

The predicted spray pattern is shown is Fig. 15. Fig. 16 shows the droplet axial velocity comparisons at two axial locations, x = 7.5 and 12.5 cm. The comparisons include the experimental results [29], our predicted results as well as those predicted results reported from the calculations of [29]. The predicted results represent the mass-averaged droplet velocities. At both axial locations, there is a decent comparison between the CFDRC and our predicted results but both mostly underestimate the experimental data in the middle. Fig. 17 shows the comparisons for the droplet radial velocities. Again, there is a good comparison between the CFDRC and our predicted results but mostly underpredict the experimental data in the middle of the spray. The average drop size (D_{32}) comparisons are shown in Fig. 18. Our results fall short of the experimental data at both axial locations but the comparisons are in reasonable agreement with the CFDRC results at the first axial location but fall short at the next axial location.

SWIRL-STABILIZED REACTING SPRAY GENERATED BY A SINGLE-ELEMENT LDI EXPERIMENT

This case is undertaken mainly to test the following models: the sheet-breakup model for primary atomization, & the TAB model for secondary droplet breakup. The experimental data for this case was provided by Cai et al [30]. It involves the modeling of a reacting spray generated by the LDI experiment. The LDI concept was developed as a part of the next generation combustor development program at NASA GRC [30]. Its aim was to achieve higher efficiency and lower combustion emissions while operating at higher engine pressures and temperatures. In the LDI approach, this was accomplished without any premixing by means of an advanced fuel injector and air swirler assembly design which ensures nearly uniform fuel and air mixing before entering the combustor.

Fig. 19 shows the test section of the experiment reported in [30]. The air passes through a six helicoidal vane swirler followed by a converging-diverging venturi before entering the combustor. The air mass flow rate is 0.49 kg/min., and at the inlet, air speed=20.4m/s, T=294.3K, P=101325Pa. The fuel nozzle is located at the middle of the centerbody and it is a Parker-Hannifin, 90-deg. hollow cone, pressure swirler. The liquid fuel is Jet-A, the liquid mass flow rate 0.025 kg/min, and the initial liquid temperature 475 K. The internal pressure drop across the atomizer is 350000 Pa which leads to an initial liquid velocity of about 22 m/s.

The results are based a 3D calculation with a grid size of 833024 elements. It makes use of the following models for the gas-phase: the standard k-epsilon turbulence model, a a single-step reduced chemical kinetic mechanism, and the eddy-breakup turbulence/chemistry model. Fig. 20 shows the spray article distribution together with the the temperature contours and the spray article distribution. The temperatures range between 400 to 2300 deg. K. The high temperature region originates downstream of the injector from the middle of the combustor and then spreads radially outwards towards the wall boundaries.

Shown in Fig. 21 are the axial velocity comparisons at six different axial locations. Although there is a qualitative comparison, the results clearly show that the predictions underestimate both the size and location of the central recirculation region. As can be seen from the first axial location, the predictions considerably overestimate the magnitude of the negative velocity at the centerline but starting from the second axial location and onwards, the predictions reverse direction and underestimate the centerline velocities. It is because the experimentally-observed central recirculation is located downstream of the predicted re-

sults. It was reported that that diverging venturi suppresses the formation of any noticeable corner vortex as it forces the outer flow to attach itself immediately next to the side wall [30]. Its effect is seen in the formation of a strong wall jet flow before hitting on the wall [30]. As a result of the ensuing flow through the corner, the axial velocity falls as seen from the location of the observed main peak and the wall boundary. However, the calculations underestimate the axial velocities in the corner region by a considerable measure. The comparisons could be improved by taking into account the unsteady nature of the flow. The comparisons for the radial velocities at different axial locations are shown in Fig. 22. Again as in the axial velocity comparisons, the comparisons are in qualitative agreement but mostly underestimate the experimental results in the first four axial locations. The high radial velocities observed at the first two axial locations near the wall could again be attributed for reasons of a strong corner flow observed in the experimental results [30]. The comparisons for the tangential velocities are shown in Fig. 23. The predictions mostly underestimate the the experimental results but provide reasonable comparison at the first axial location.

Fig. 24 shows the comparisons for the Sauter mean droplet sizes (d_{32}). There is a good comparison in general. It is interesting to note that droplets start to disappear from the central region and the spray develops into a doughnut-shape further downstream as seen in the last two axial locations. It is because most of the smaller droplets start to disappear after vaporizing from the middle, where gas temperatures start to rise because of combustion, while the larger droplets move radially outwards. It is also intersting to note that the droplet distribution becomes more uniform at the last two axial locations. It is because as the smaller droplets start to vaporize more quickly, it leaves the remaining distribution with a more fairly uniform large-size droplets.

Fig. 25 Shows the droplet mean axial velocity comparisons at six different axial locations. Shown are the predicted results as well as the experimental data for two different droplet-size groups: 0-15 microns and 60-75 microns. The data for the 0-15 microns represent the velocities of the smallest droplet-size group and the data for the 60-75 microns represent the velocities of the largest droplet-size group. Our calculations are based on the mean-size droplet representation and as such the predicted sizes are expected to fall closer to the 60-75 microns size group

and are also expected to fall between the two droplet-size groups. The comparisons are mostly in good agreement and fall mostly closer to the large-size droplet group. However, there is some underestimation in the middle of the first axial location and in the outer region of the second axial location. It is noteworthy that the radial spreading rate of the spray is well predicted.

Fig. 26 shows the droplet radial velocity comparisons. Again there is a good agreement between the predicted and the experimental results of the large-size droplets. However, there is some underestimation in the middle of the first axial location and in the outer regions of the second and third axial locations. It is also interesting to note that radial velocities for the small-size droplets are much higher than the corresponding larger-size droplets in the first two axial locations. It is because the smaller droplets tend to follow closer to the gas velocity where the radial velocities are higher as evidenced in Fig. 22. The droplet mean tangential velocity comparisons are shown in Fig. 27. The predicted results are closer to the experimental data of the large-size droplets at the first two axial locations. The calculations mostly underpredict the experimental results in the next four locations. In determining the initial droplet tangential velocities, no swirl component was specified. Perhaps, the comparisons could be improved by providing an additional swirl component to the initial liquid velocity.

CONCLUDING REMARKS

Here we provide a summary of our validation results involving both superheated and non-superheated liquid sprays.

(1) We have studied the two-phase jet characteristics of a superheated spray generated by the sudden release of pressurized R134A from a cylindrical nozzle. The predicted profiles for both gas and droplet velocities show a reasonable agreement with the measured data. They exhibit a self-similar pattern as given by a correlation reported in the literature. There is a need for improvement in the atomization modeling when it comes to the droplet-size comparisons for the following reasons: the experimental data show a much wider radial variation in the droplet sizes when compared with the predictions but the predictions manage to calculate the overall SMD with a reasonable accuracy, the predicted droplet sizes mainly fall short of experimental data

in the central region of the spray, and the predicted sizes are in reasonable agreement with the experimental behavior away from the central region. Both the predictions and experimental data show that a considerable amount of vaporization takes place under non-superheated conditions. Since we can't make direct comparisons with the hot-wire temperature measurements, there is a need for more data on separate gas and liquid temperatures for a proper validation of the vaporization models used in our present study.

(2) Our second validation involves the modeling of a liquid jet atomizing in a subsonic cross-flow based on a 3D calculation (non-reacting & turbulent air-flow). This investigation is undertaken mainly to test the following models: BLS or blob-jet for primary atomization & ETAB for secondary droplet breakup. The results (droplet size and velocity) from the blob-jet model are in reasonable agreement with the experimental data. However, the results from the BLS model are found to be slightly less favorable.

(3) Our third validation involves the modeling of a liquid spray generated by a pressure swirl atomizer based on an axisymmetric calculation (non-reacting & turbulent air-flow). This investigation is undertaken mainly to test the following models: the sheet-breakup model for primary atomization, & the ETAB model for secondary droplet breakup. The comparisons include mean droplet axial and radial velocities and average droplet sizes (D_{32}). The predicted results are in reasonable agreement with the predicted CFDRC results but mostly underestimate the experimental data.

(4) Our fourth validation involves the modeling of a reacting spray generated by a single element LDI experiment based on a 3D calculation (turbulent air-flow). This investigation is undertaken mainly to test the following models: the sheet-breakup model for primary atomization, & the ETAB model for secondary droplet breakup. The predicted gas-phase results underestimate both size and location of the central recirculation region but the predictions provide better agreement for the droplet size and droplet velocities.

REFERENCES

1. M.S. Raju, LSPRAY-III: A Lagrangian Spray Module, NASA/CR–2008-215290, NASA Glenn Research Center, Cleveland, Ohio, July 2008.

2. M.S. Raju, EUPDF-II: An Eulerian Joint Monte Carlo PDF Module, NASA/CR–2004-213073, NASA Glenn Research Center, Cleveland, Ohio, April, 2004.

3. Raju, M.S., "CFD Modeling of Superheated Sprays," AIAA-2009-1187, the 47th Aerospace Sciences Meeting, Orlando, Florida, January 5-8, 2009.

4. Raju M.S., and Sirignano, W.A., "Multi-Component Spray Computations in a Modified Centerbody Combustor," Journal of Propulsion and Power, Vol. 6, No. 2, March-April 1990.

5. Raju, M.S., "AGNI-3D: A Computer Code for the Three-Dimensional Modeling of a Wankel Engine," Computers in Engine Technology, Proceedings IMechE, London, United Kingdom, pp. 27-37, 1991.

6. Raju, M.S., "Heat Transfer and Performance Characteristics of a Dual-Ignition Wankel Engine," Journal of Engines, the 1992 SAE Transactions, Section 3, pp. 466-509.

7. M.S. Raju, Application of Scalar Monte Carlo Probability Density Function Method For Turbulent Spray Flames, Numerical Heat Transfer, Part A, vol. 30, pp. 753-777, 1996.

8. M.S. Raju, Current Status of the Use of Parallel Computing in Turbulent Reacting Flows: Computations Involving Sprays, Scalar Monte Carlo Probability Density Function & Unstructured Grids, Advances in Numerical Heat Transfer, vol. 2, ch. 8, pp.259-287, 2000.

9. M.S. Raju, Scalar Monte Carlo PDF Computations of Spray Flames on Unstructured Grids With Parallel Computing, Numerical Heat Transfer, Part B, No. 2, Vol. 35, pp. 185-209, March 1999.

10. M.S. Raju, On the Importance of Chemistry/Turbulence Interactions in Spray Computations, Numerical Heat Transfer, Part B: Fundamentals, No. 5, Vol. 41, pp. 409-432, 2002.

11. Lucas, K.D., Tseng, C.C., Pourpoint, T.L., Lucht, R.P., and Anderson, W.E., "Imaging Flashing Injection of Acetone at Jet Engine Augmentor Conditions," AIAA Paper 2007-1182, 45th AIAA Aerospace Sciences Meeting and Exhibit, Reno, Nevada, Jan. 8-11, 2007.

12. Zuo, B., Gomes, A.M., and Rutland, C.J., "Modeling Superheated Fuel Sprays and Vaporization," Int. J. Engine Research, vol. 1, no. 4, pp. 321-336.

13. Yildiz, D., Rambaud, P., Van Beeck, J., Buchlin, J.-M., "Characterization of Superheated Liquid Jet Atomization Phase Doppler Anemometer (PDA) and High-Speed Imaging," Proceedings of FEDSM2006: 2006 ASME Joint U.S.-European Fluids Engineering Summer Meeting, July 17-20, 2006, Miami, Florida.

14. Yildiz, D., Rambaud, P., Van Beeck, J., Buchlin, J.-M., "Evolution of the Spray Characteristics in Superheated Liquid Jet Atomization in Function of Initial Flow Conditions," ICLASS-2006, Paper ID ICLASS06-122, Aug. 27-Sept 1, 2006, Kyoto, Japan.

15. Schmehl, R, and Steelant, J., "Flash-Evaporation of Oxidizer During Start-Up of an Upper-Stage Rocket Engine," AIAA Paper 2003-5075, 39th AIAA/ASME SAE/ASEE Joint Propulsion Conference and Exhibit, Huntsville, Alabama, July 20-23 2003.

16. Schmehl, R, and Steelant, J., "Evaluation of Oxidizer Temperature Drop in a Combustion Chamber," 4th International Conference on Launcher Technology "Space Launcher Liquid Propulsion, Liege, Belgium, December 3-6 2002.

17. Adachi, M., McDonnel, V.G., Tanaka, D., Senda, J, and Fujimoto, H., "Characteristics of Fuel Vapor Concentration Inside a Flash Boiling Spray," SAE Paper 970871, 1997.

18. Lucas, K.D., Tseng, C.C., Pourpoint, T.L., Lucht, R.P., and Anderson, W.E., "Imaging Flashing Injection of Acetone at Jet Engine Augmentor Conditions," AIAA Paper 2007-1182, 45th AIAA Aerospace Sciences Meeting and Exhibit, Reno, Nevada, Jan. 8-11, 2007.

19. Lefebvre, A., "Atomization and Sprays," Hemisphere Publishing Company, New York, pp. 165-222, 1989.

20. VanDerWege, B.A., Lounberry, T.H., and Hochgreb, S., "Numerical Modeling of Fuel Sprays in DISI engines Under Early-Injection Operating Conditions," SAE Paper 2000-01-0273, 2000.

21. Reitz, R.D., "A Photographic Study of Flash-Boiling Atomization," Aerosol Science Technology, Vol, 12, pp. 561-569, 1990.

22. Yildiz, D., Rambaud, P., Van Beeck, J., Buchlin, J.-M., "A Study on the Dynamics of a Flashing Jet," Von Karman Institute for Fluid Mechanics, Final Contract Research Report-EAR0030/2002.

23. "CFD Modeling of Flashing Jet Dispersion," Fluids Mechanics Research Group, University of Hertfordshire, United Kingdom, FLIE Report-Feb. 2005.

24. Hetsroni, G., and Sokolov, M., "Distribution of Mass, Velocity, and Intensity of Turbulence in a two-phase Turbulent Jet," J. Appl. Mech., vol. 32, pp.315, 1971.

25. Pope, S.B., "Turbulent Flows," Cambrige University Press, 2000.

26. Bayvel, L.P., and Orzchowski, Z, " Liquid Atomization," Taylor & Francis, Combustion: An International Series, !st edition, 1993.

27. Reitz, R.D., "Modeling Atomization Processes in High-Pressure vaporizing Sprays," Atomization and Spray Technology, Vol. 3, pp. 309-337, 1987.

28. Wu, P.-K., Kirkendall, K.A., and Fuller, R.P., "Spray Structures of Liquid Jets Atomized in Subsonic Crossflows," Journal of Propulsion and Power, vol.14, No.2, pp. 173-182, March-April, 1998.

29. Benjamin, M.A., and Crocker, D.S., "Spray Characterization of a Relatively High Flow Simplex Atomizer Using Experiment and CFD," 32th Joint Propulsion Conference, AIAA paper 96-3165, July 1996.

30. Cai, J., Jeng, S.-M., & Tacina, R., "The Structure of a Swirl-Stabilized Reacting Spray Issued From an Axial Swirler," 43rd AIAA Aerospace Sciences Meeting & Exhibit, AIAA 2005-1424, January 2005.
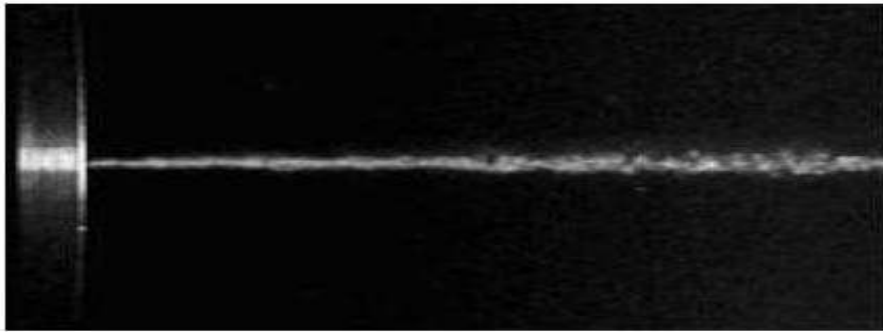
Fig. 1 R134–A Jet under 700 kPa at 23 deg. C for the 1mm nozzle
(taken from Yildiz et al [22])
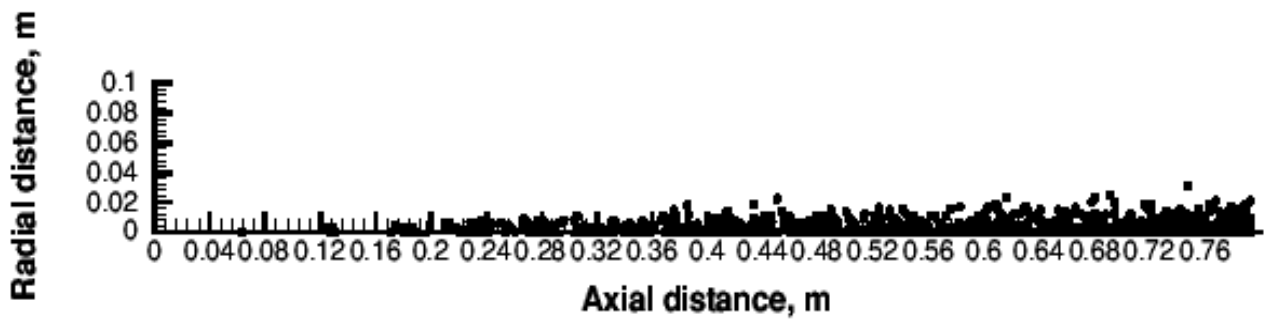
Fig. 2 An axisymmetric view of the predicted spray pattern from
Calculation 1.
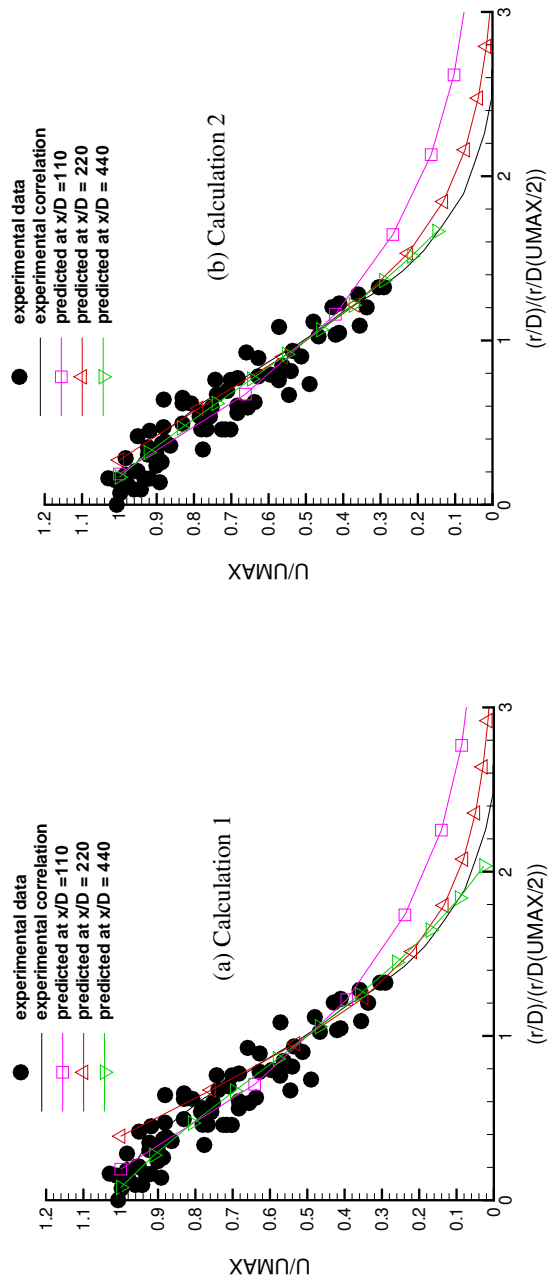
Fig. 3a-b Gas velocity comparisons from Calculations 1 & 2 of the VKI validation case.
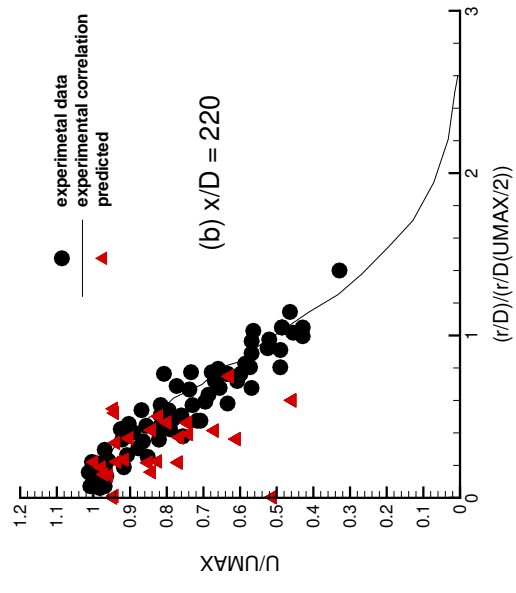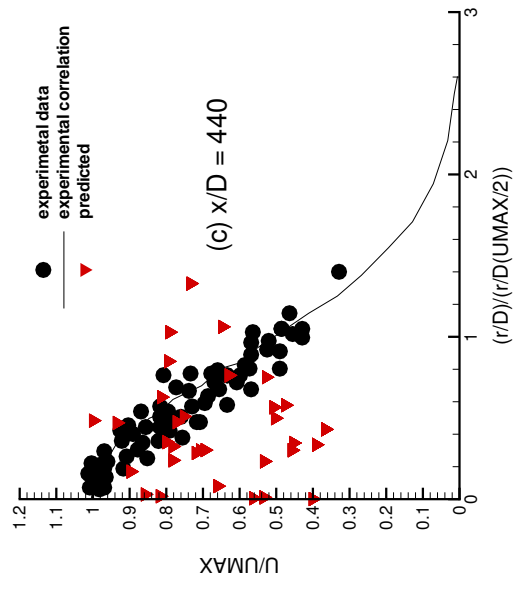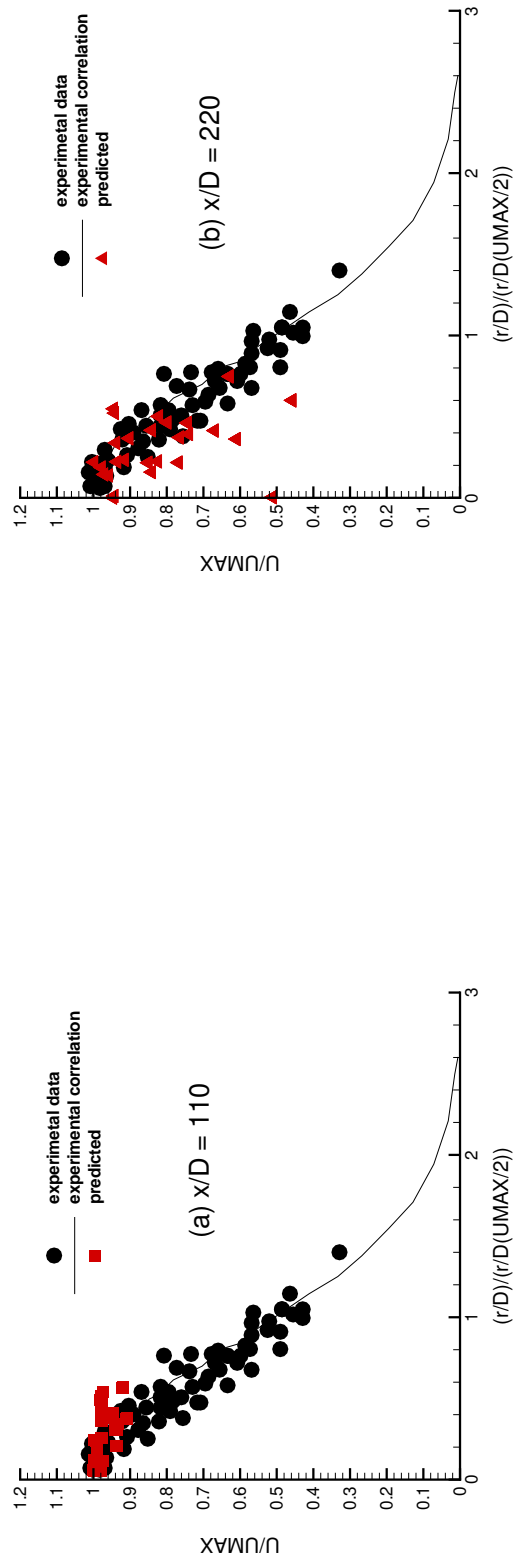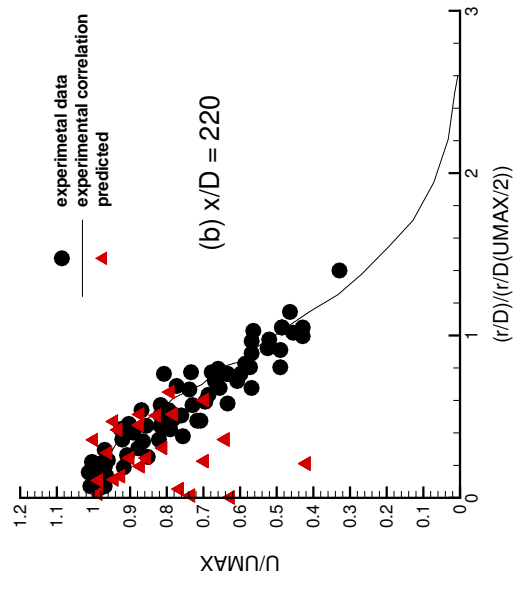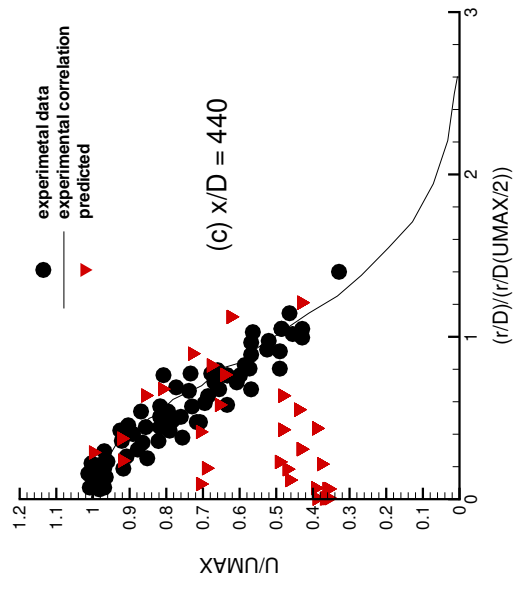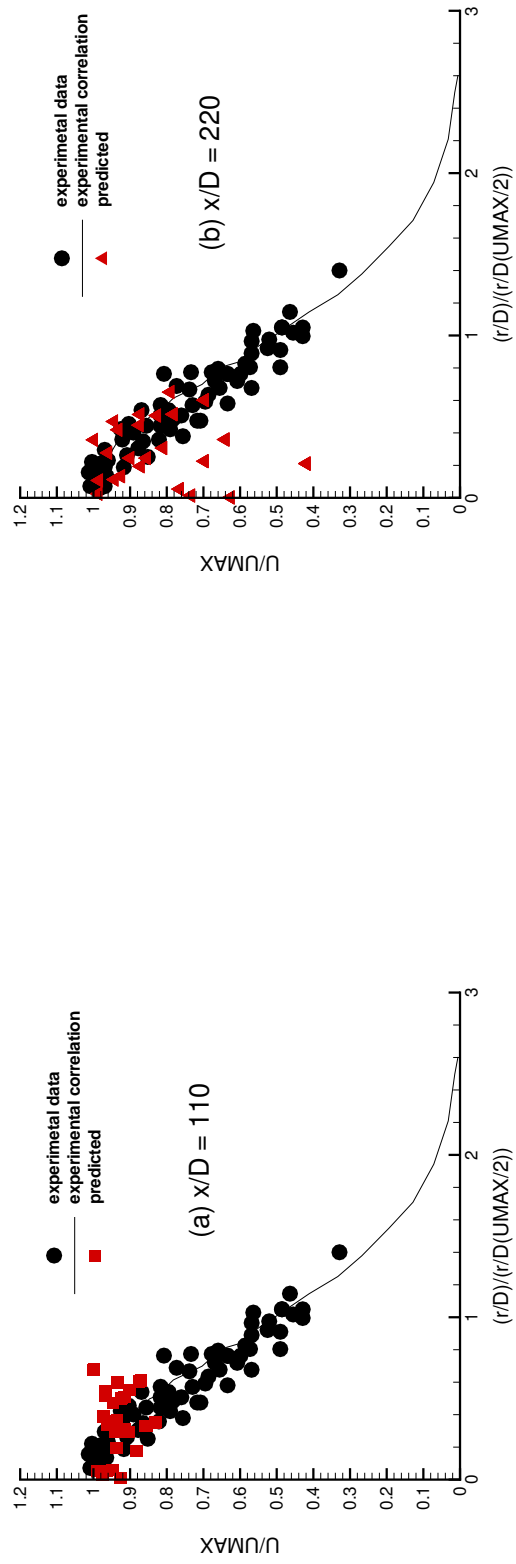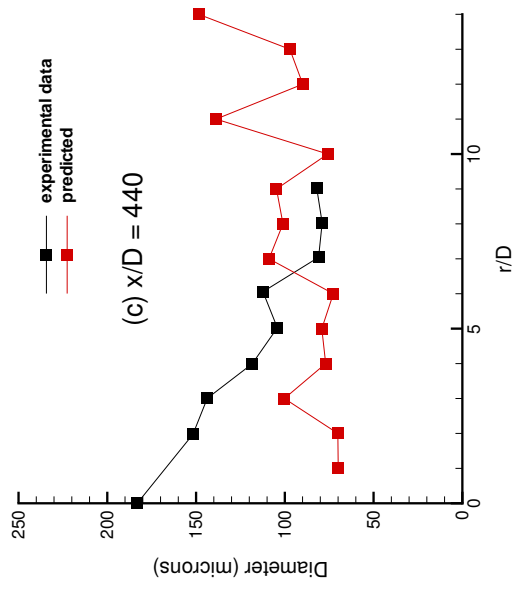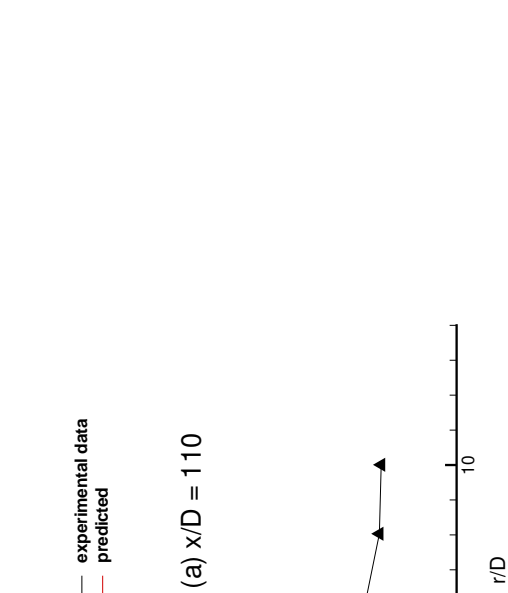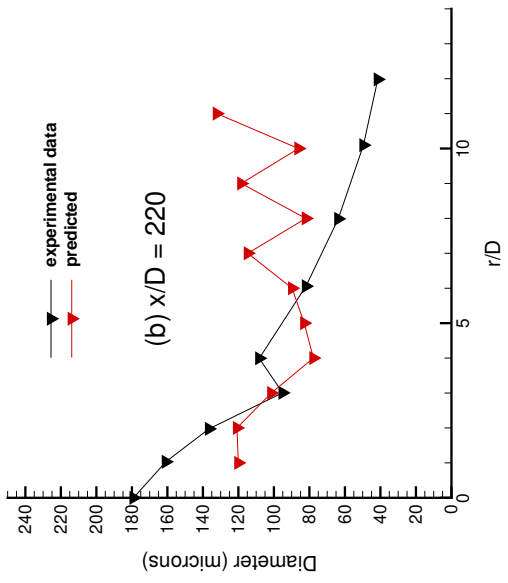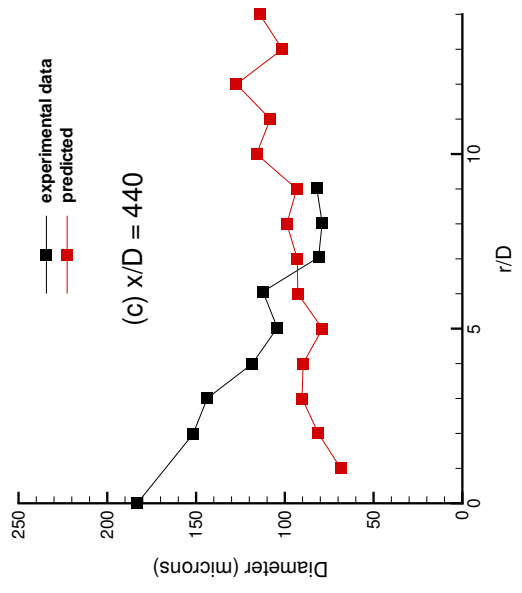
Fig. 4a-c Droplet velocity comparisons at three axial locations from Calculation 1 of the VKI validation case.

Fig. 5a-c Droplet velocity comparisons at three axial locations from Calculation 2 of the VKI validation case.

Fig. 6a-c Mean droplet size comparisons at 3 axial locations from Calculation 1 of the VKI validation case.
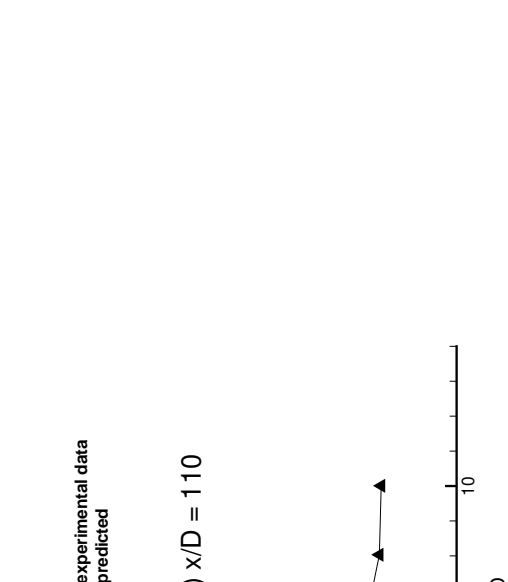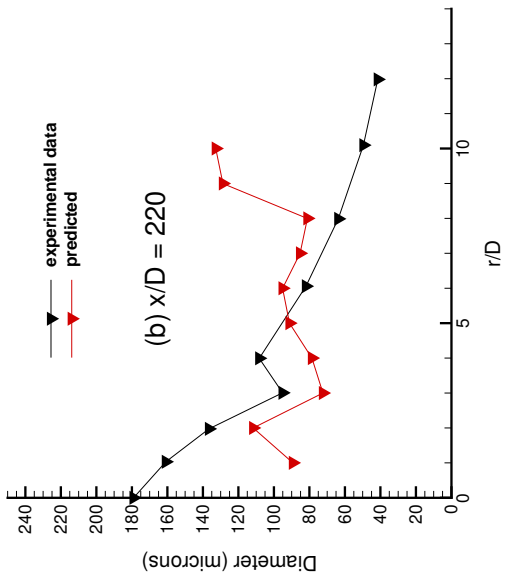
Fig. 7a-c Mean droplet size comparisons at 3 axial locations from Calculation 2 of the VKI validation case.
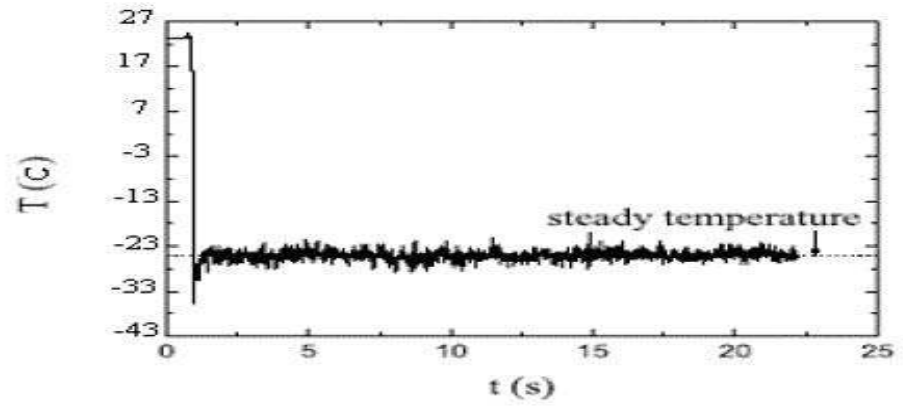
Fig. 8 Temperature signal in time from the thermocouple
measurement (taken from Yildiz et al [22])
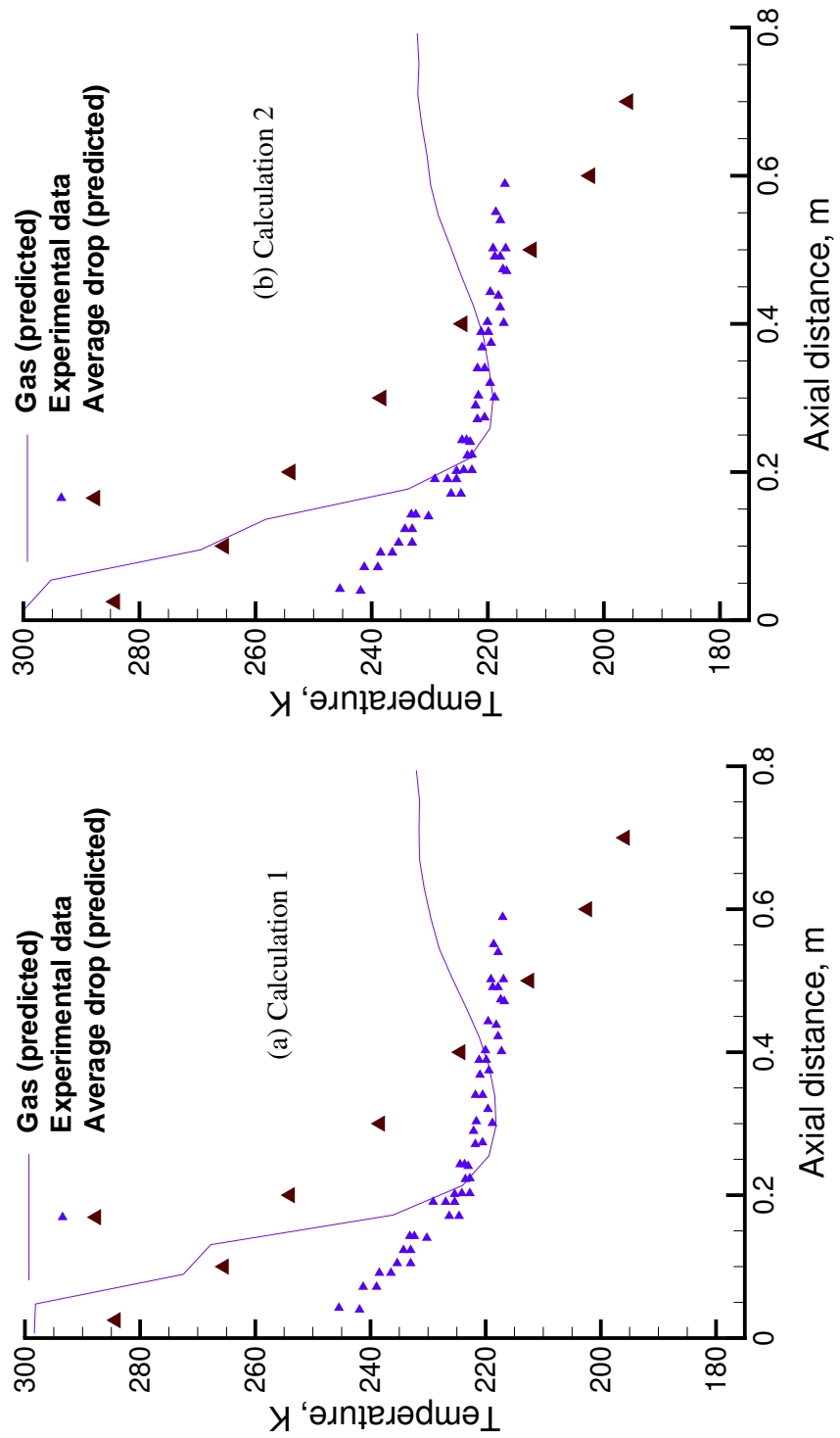
Fig. 9a-b Axial variation of temperature near the centerline from Calculations 1 & 2 of the VKI validation case.
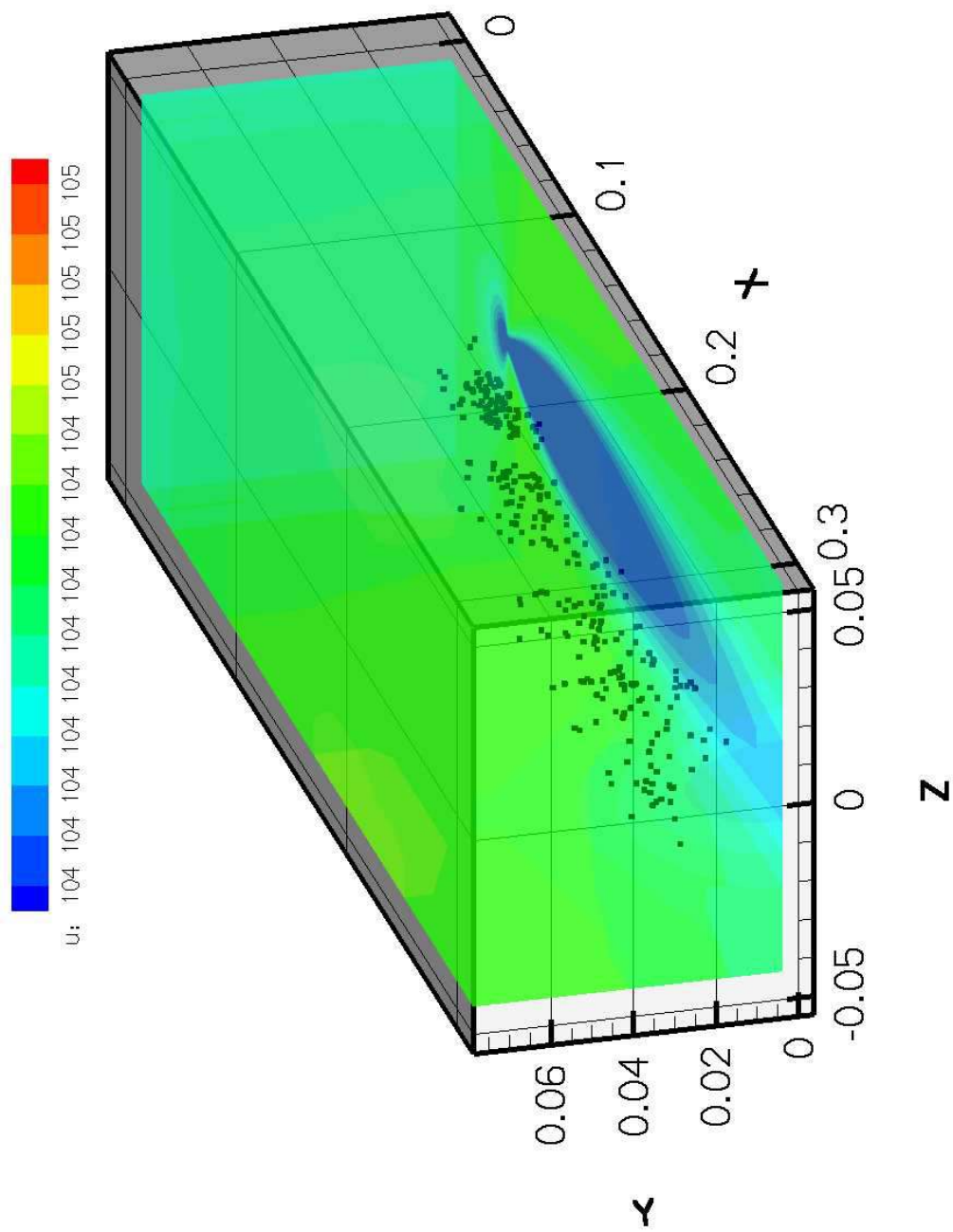
Fig. 10 A three-dimensional perspective view of the liquid jet in a cross flow.
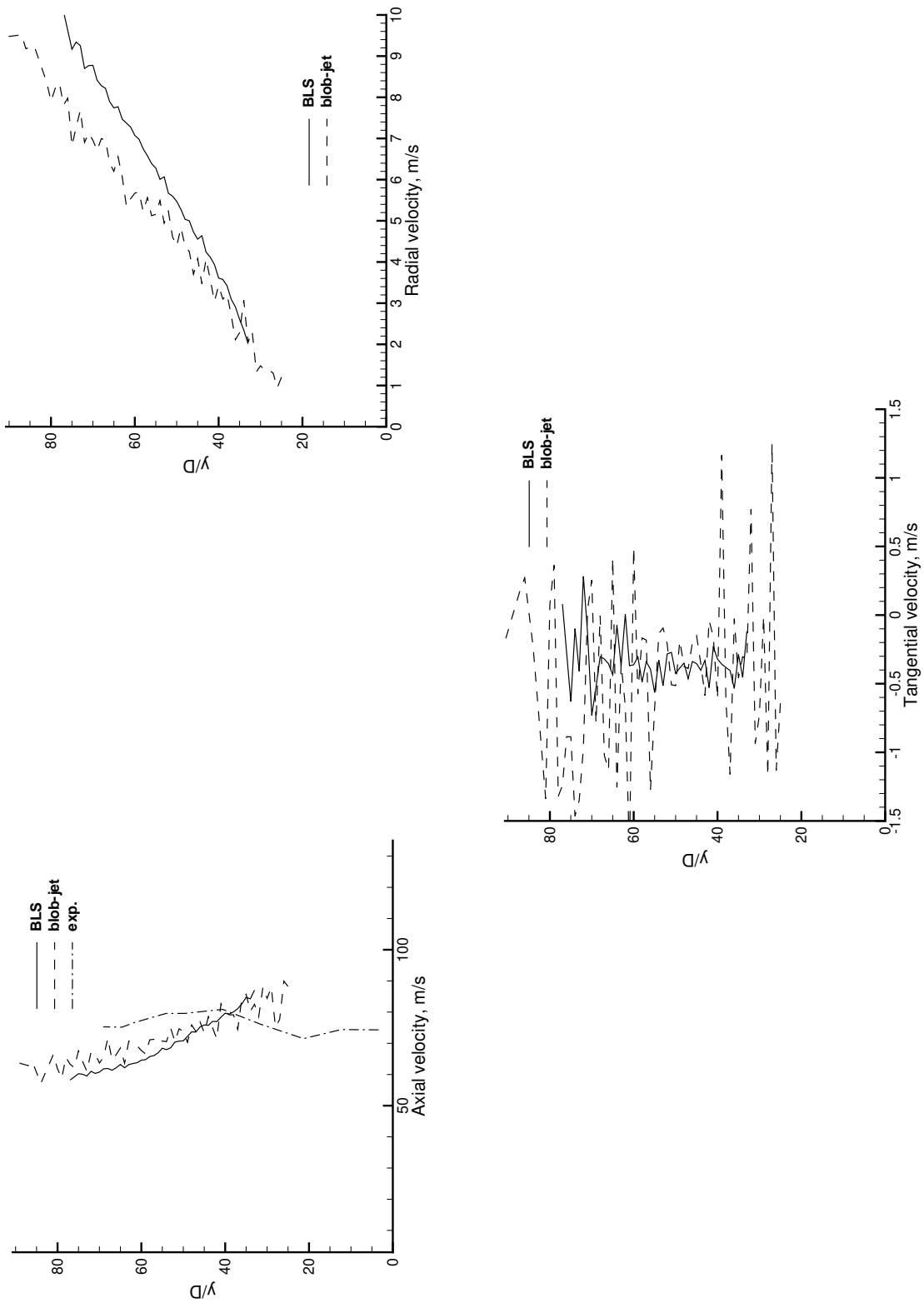
Fig. 11 Droplet velocity comparisons at x/D =200 for the liquid jet in a cross flow.
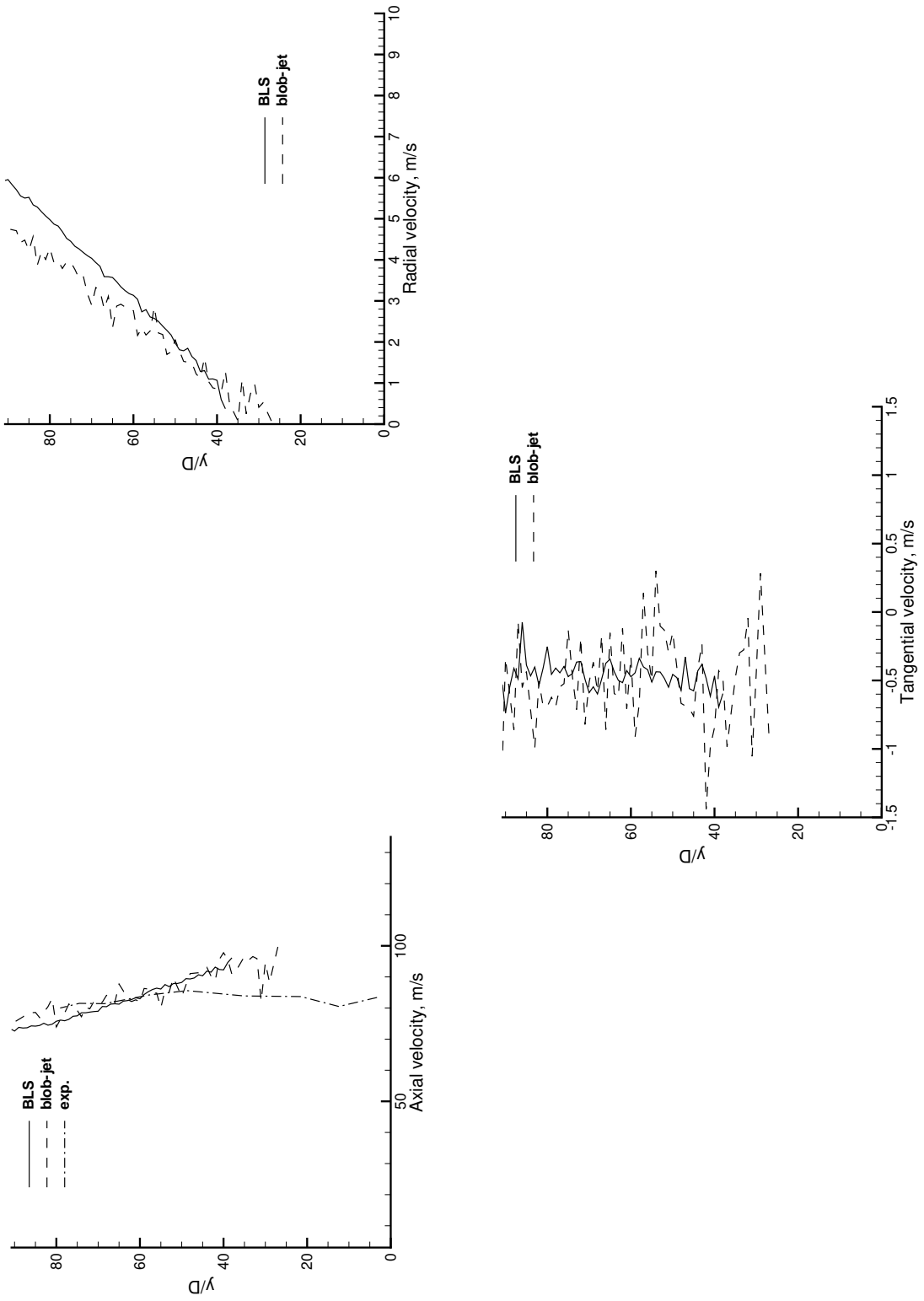
Fig. 12 Droplet velocity comparisons at x/D =300 for the liquid jet in a cross flow.
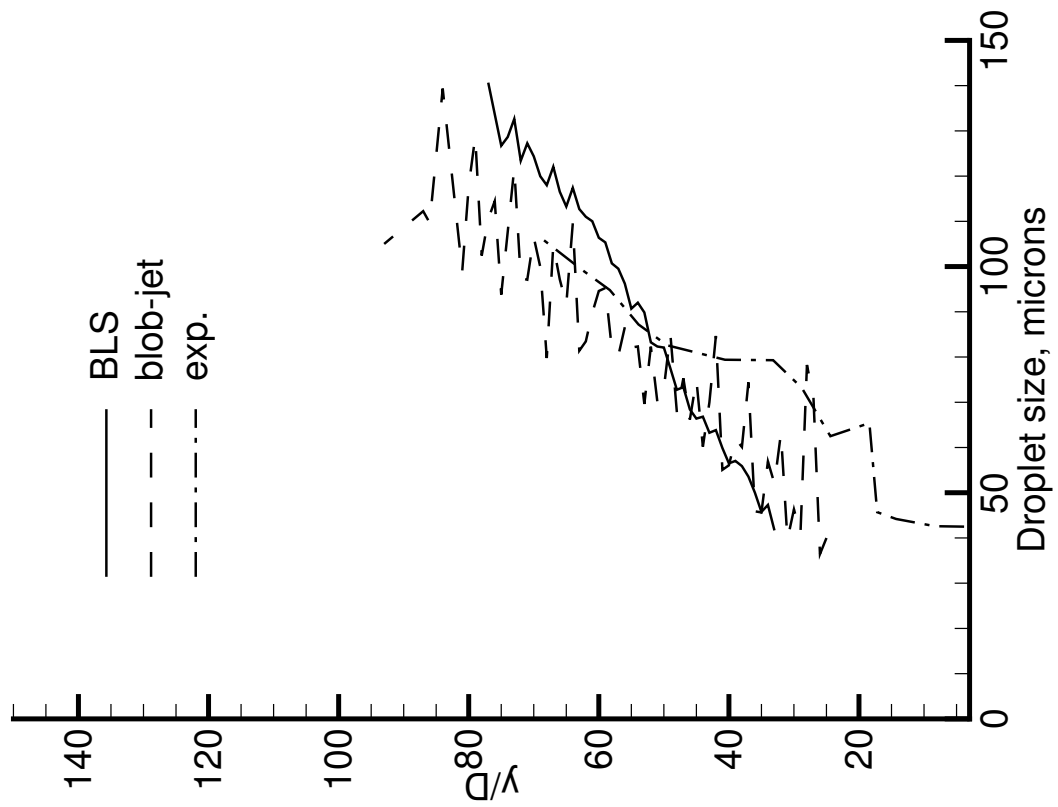
Fig. 13 Droplet size comparisons at x/D=200 for the liquid jet in a cross flow.
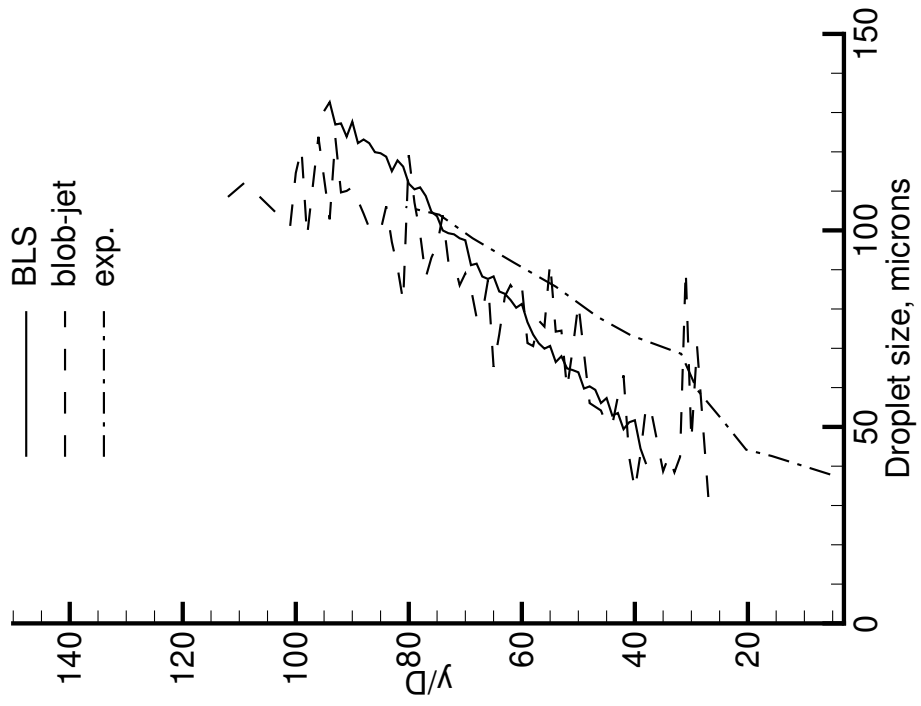
Fig. 14 Droplet size comparisons at x/D=300 for the liquid jet in a cross flow.
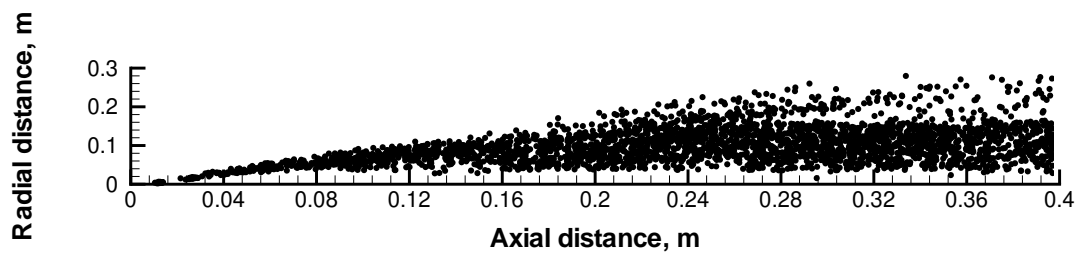
Fig. 15 Predicted spray pattern for the Parker-Hannifin validation case.
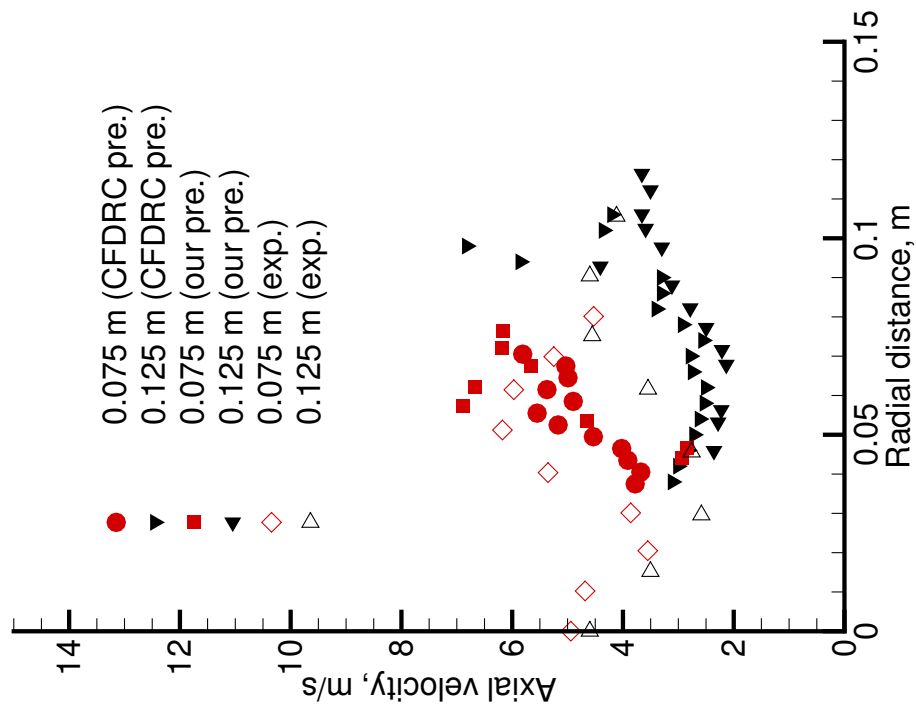
Fig. 16 Axial droplet velocity comparisons for the Parker-Hannifin validation case.
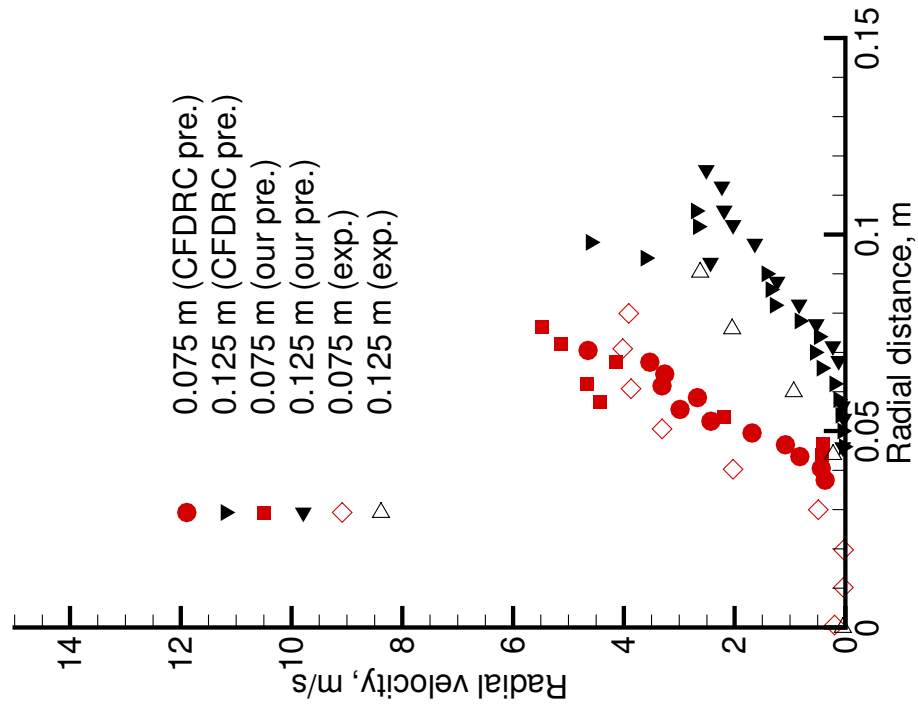
Fig. 17 Radial droplet velocity comparisons for the
Parker-Hannifin validation case.
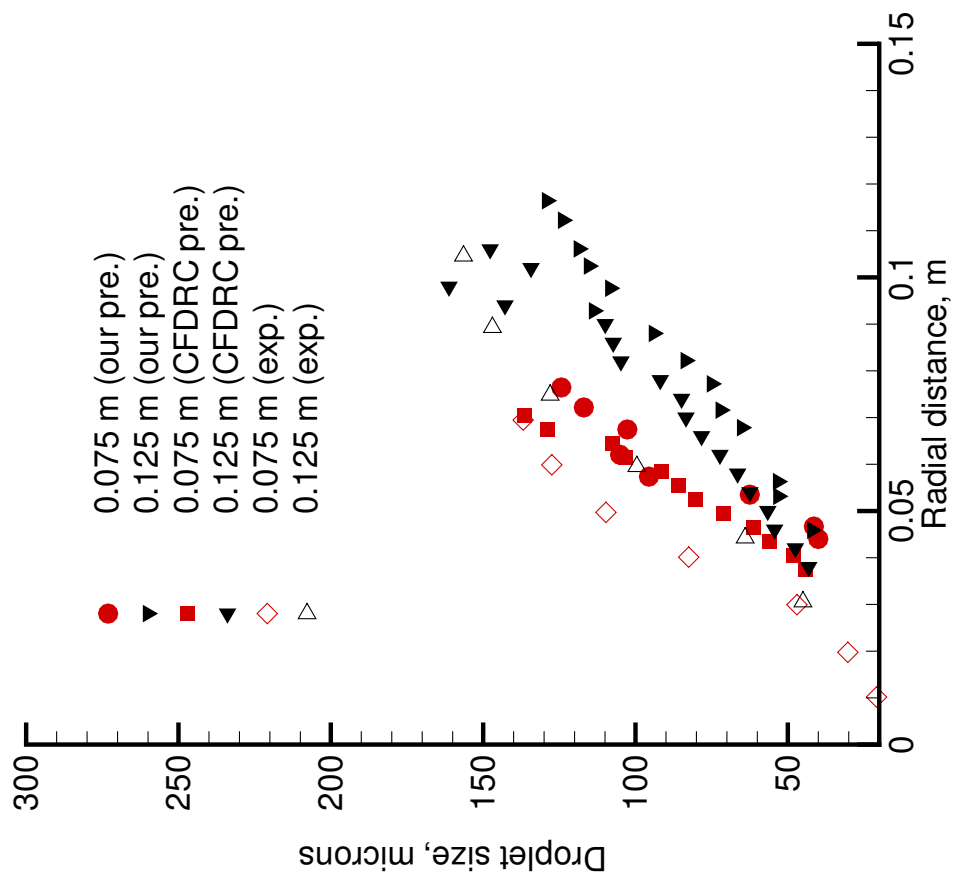
Fig. 18 Droplet size comparisons for the Parker-Hannifin validation case.
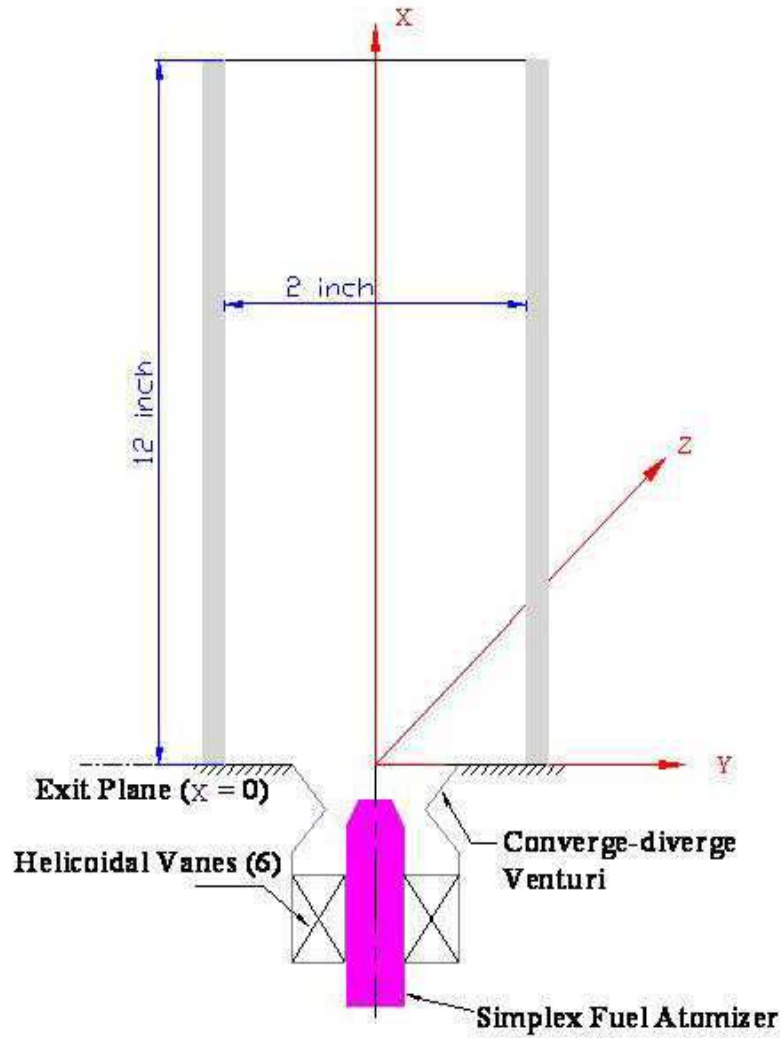
Fig. 19 Test setup of the single−element LDI experiment
(taken from Cai et al [30]).
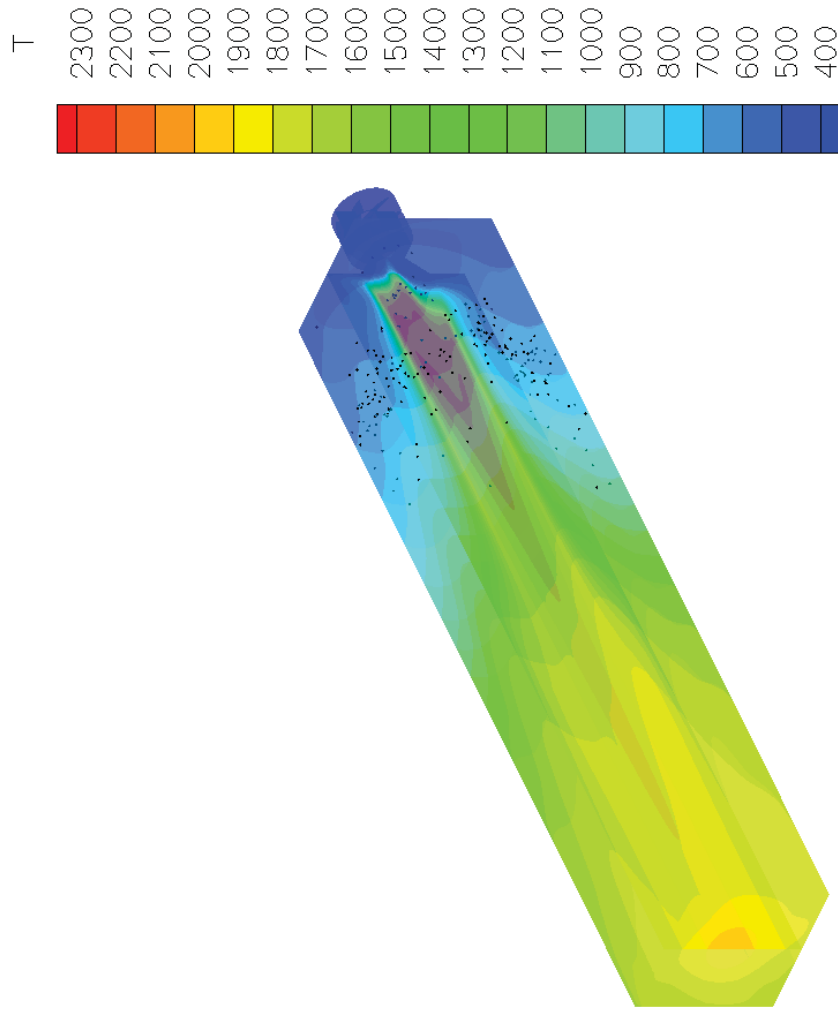
Fig. 20 A 3D perspective view of the reacting spray generated by the single-element LDI experiment.
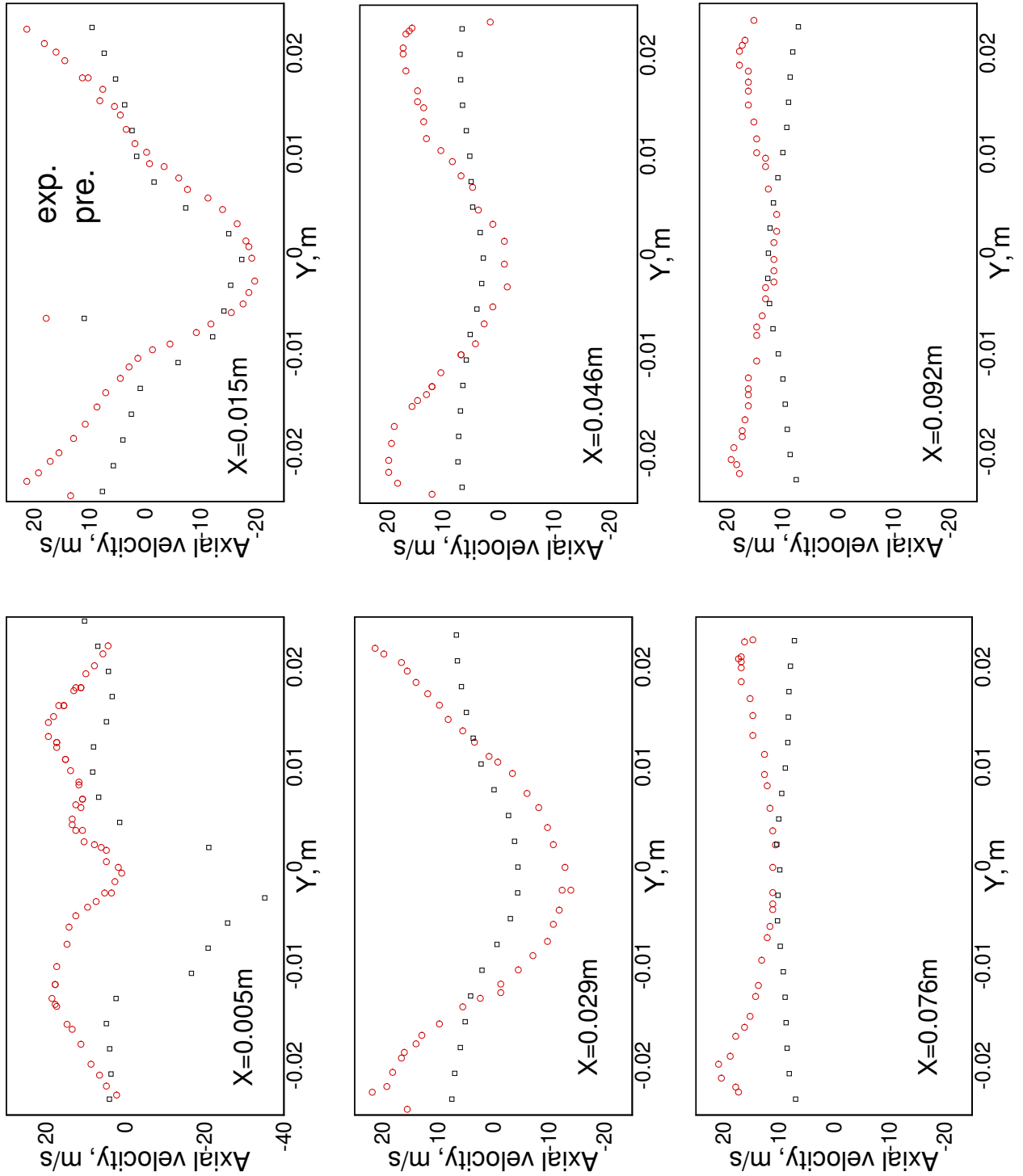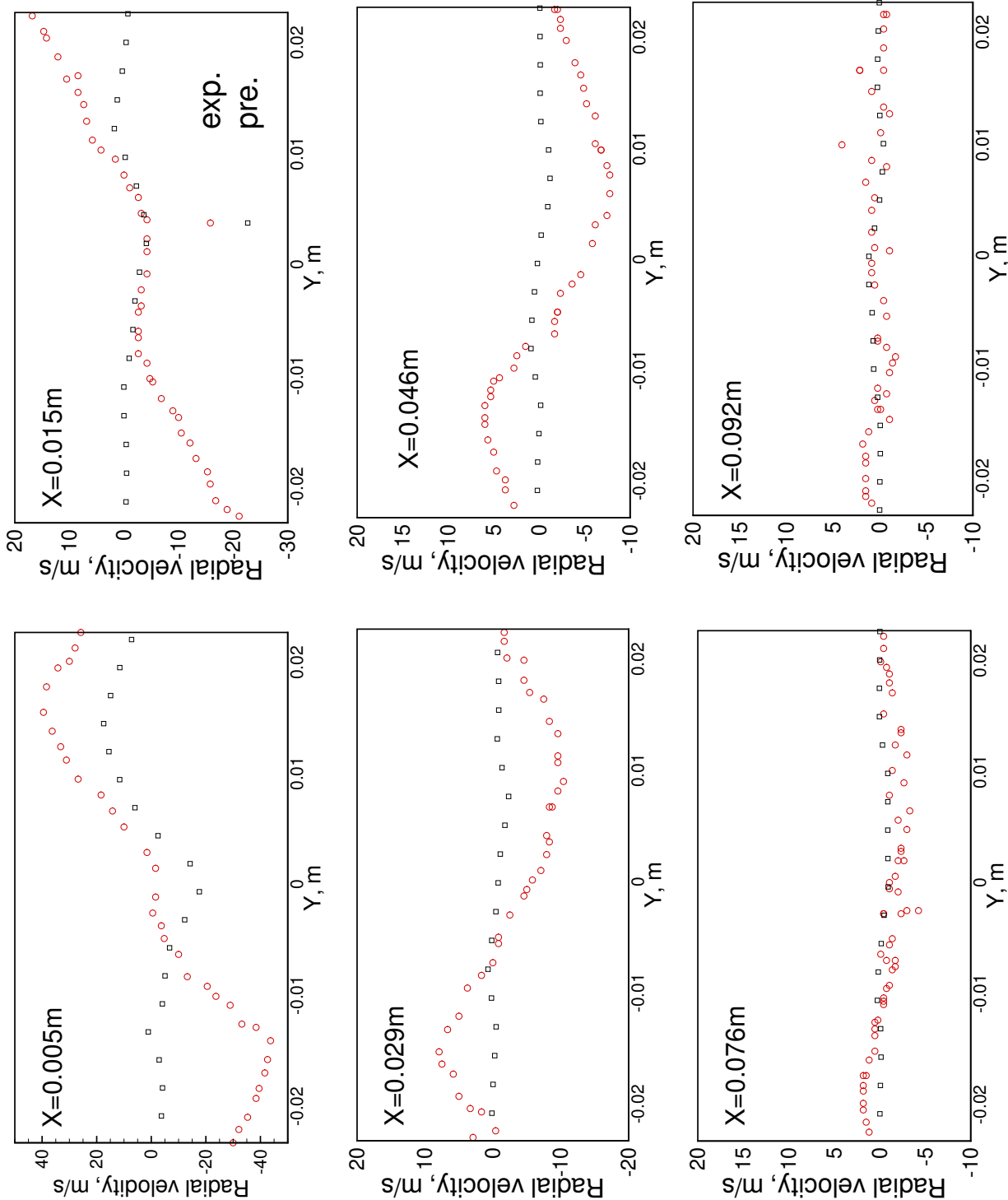
Fig. 21 Gas mean axial velocity distributions.
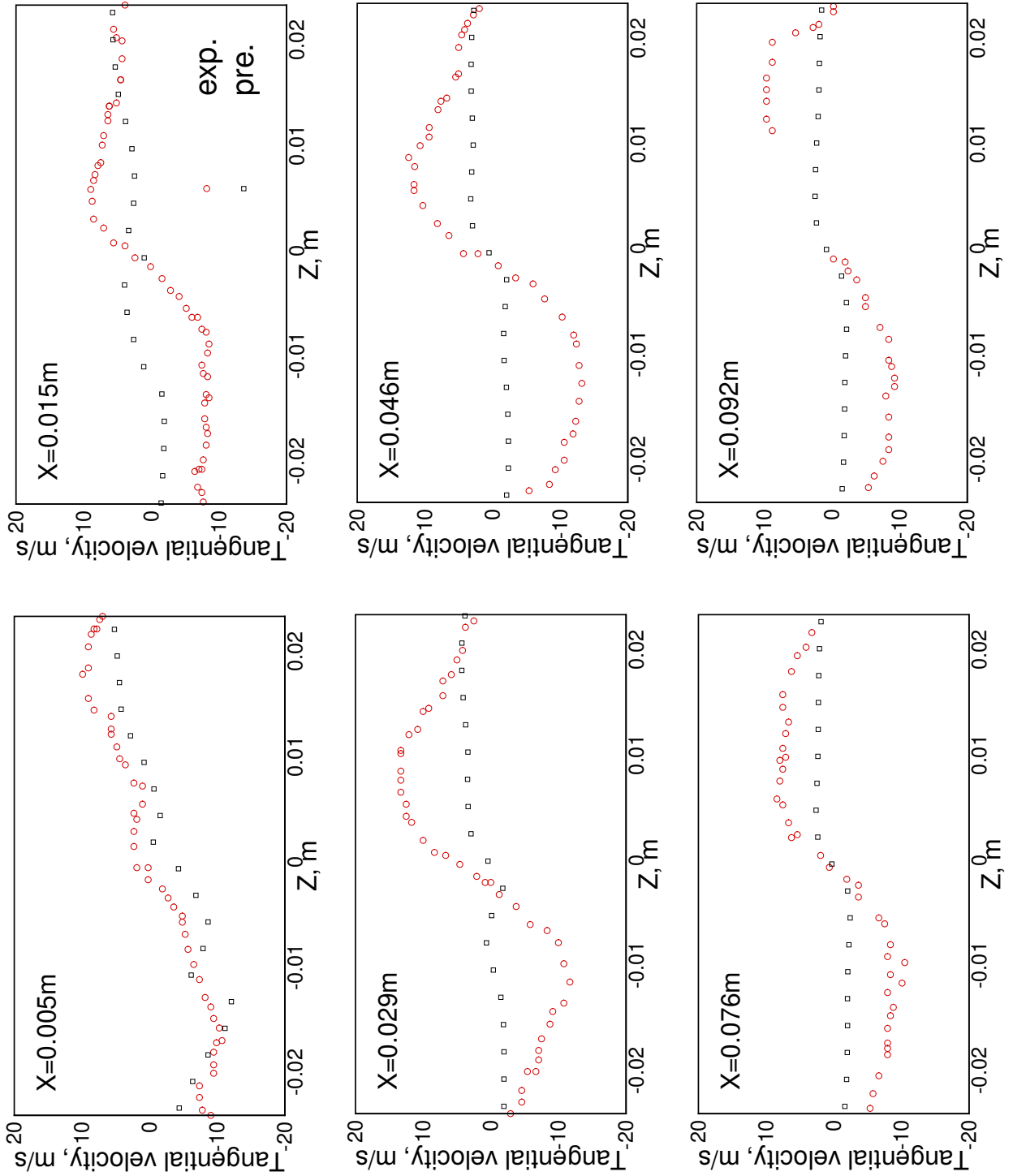
Fig. 22 Gas mean radial velocity distributions.

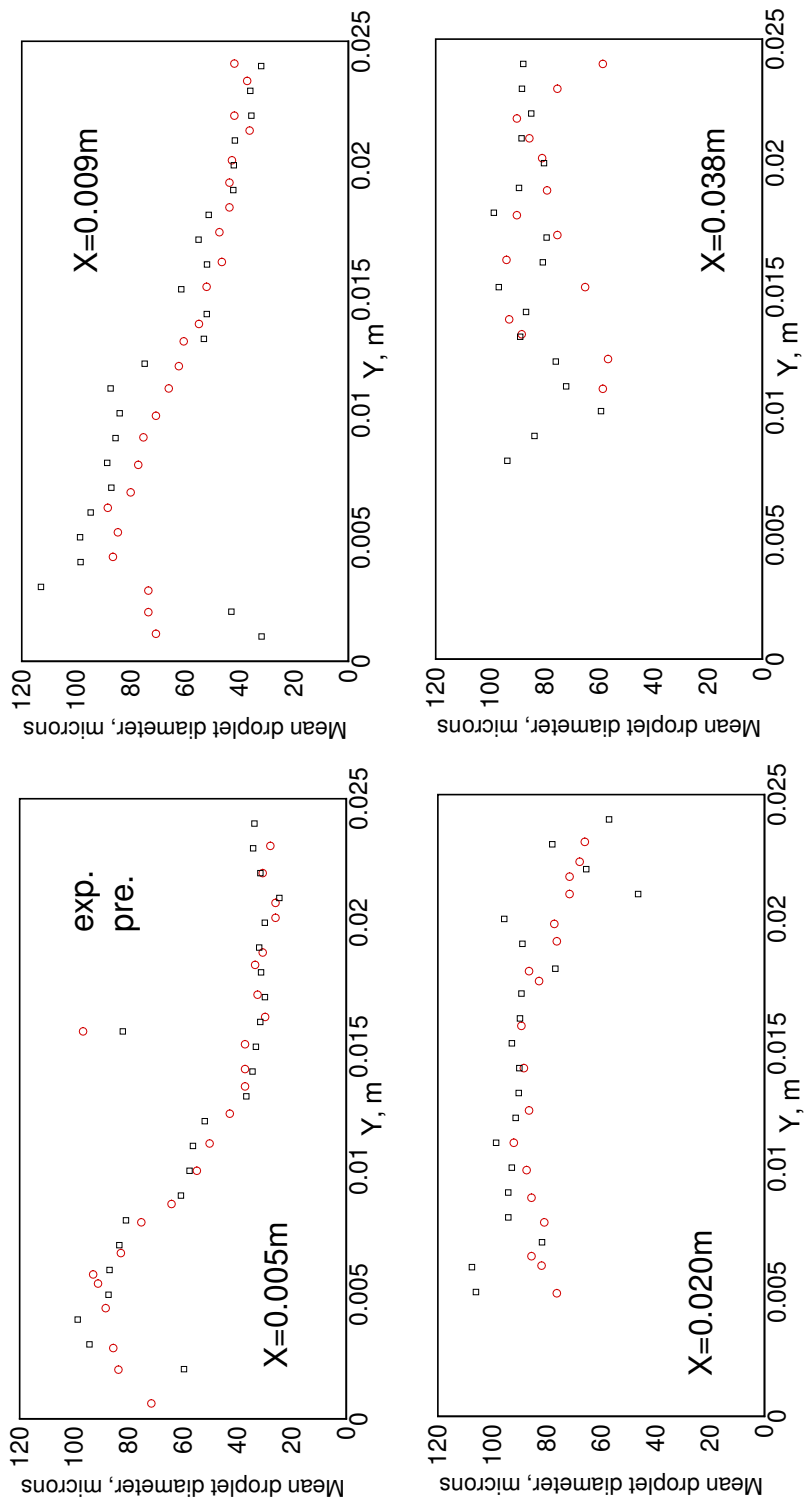Fig. 23 Gas mean tangential velocity distributions.

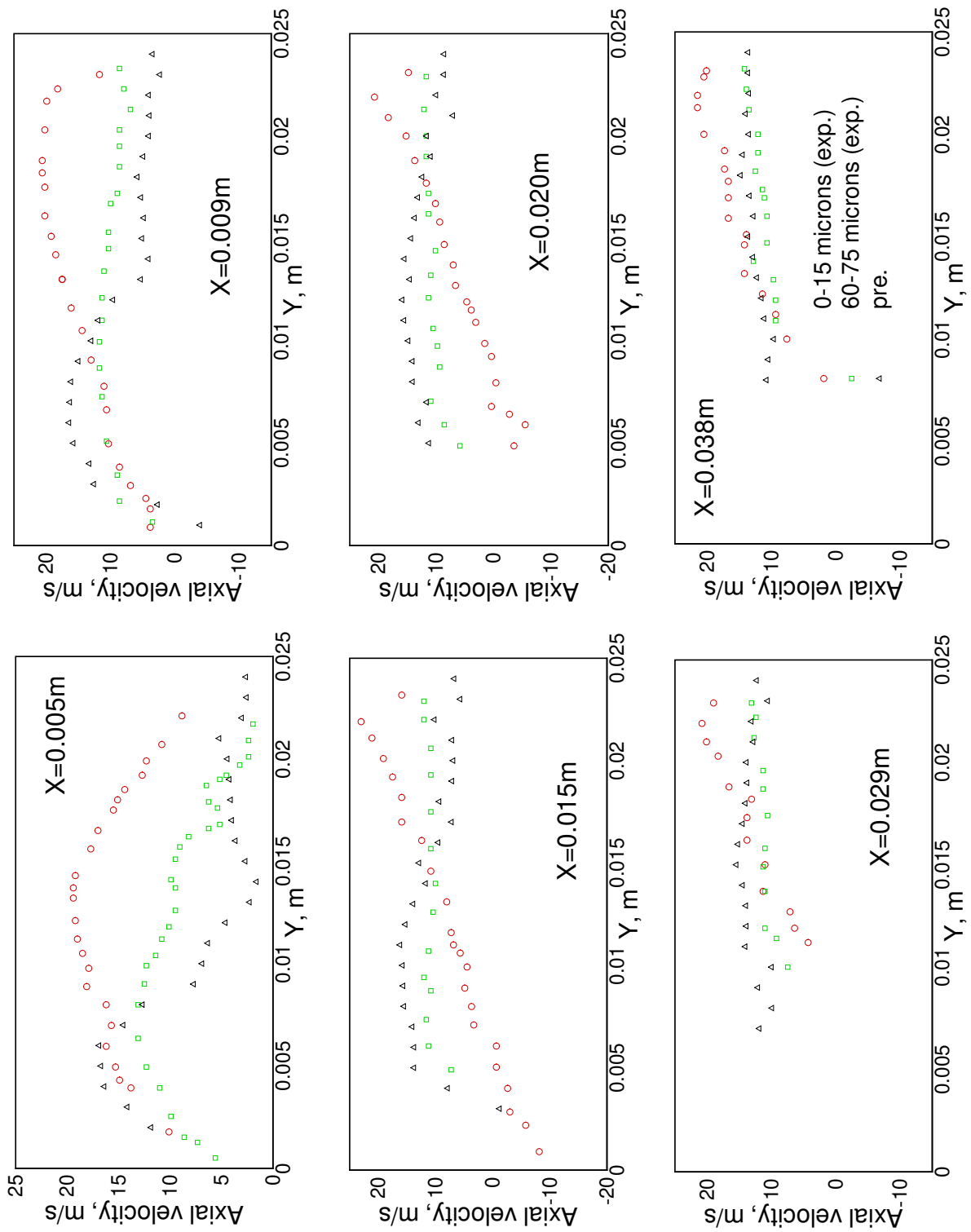Fig. 24 Mean droplet diameter (D32) distributions.
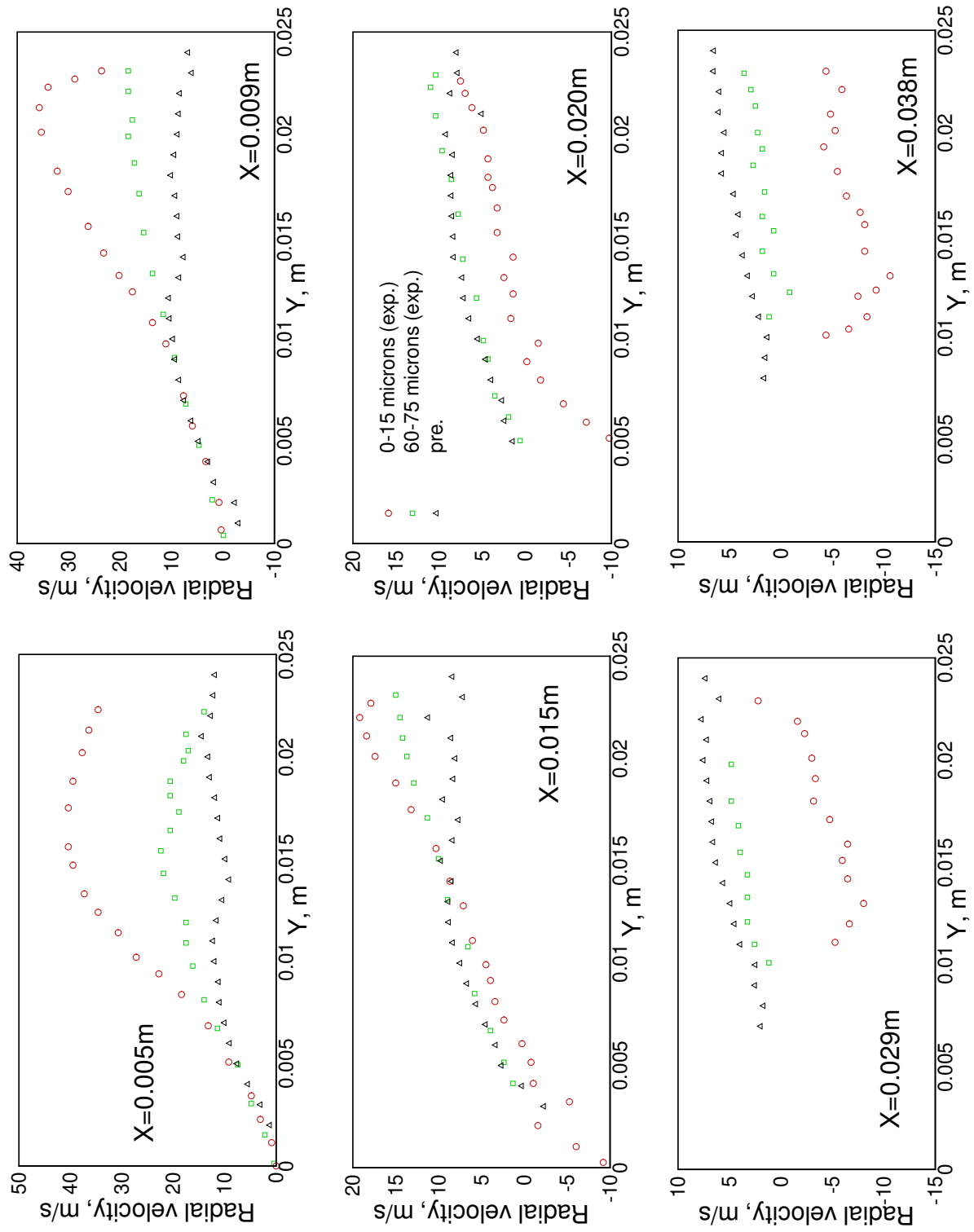
Fig. 25 Spray mean axial velocity distributions.

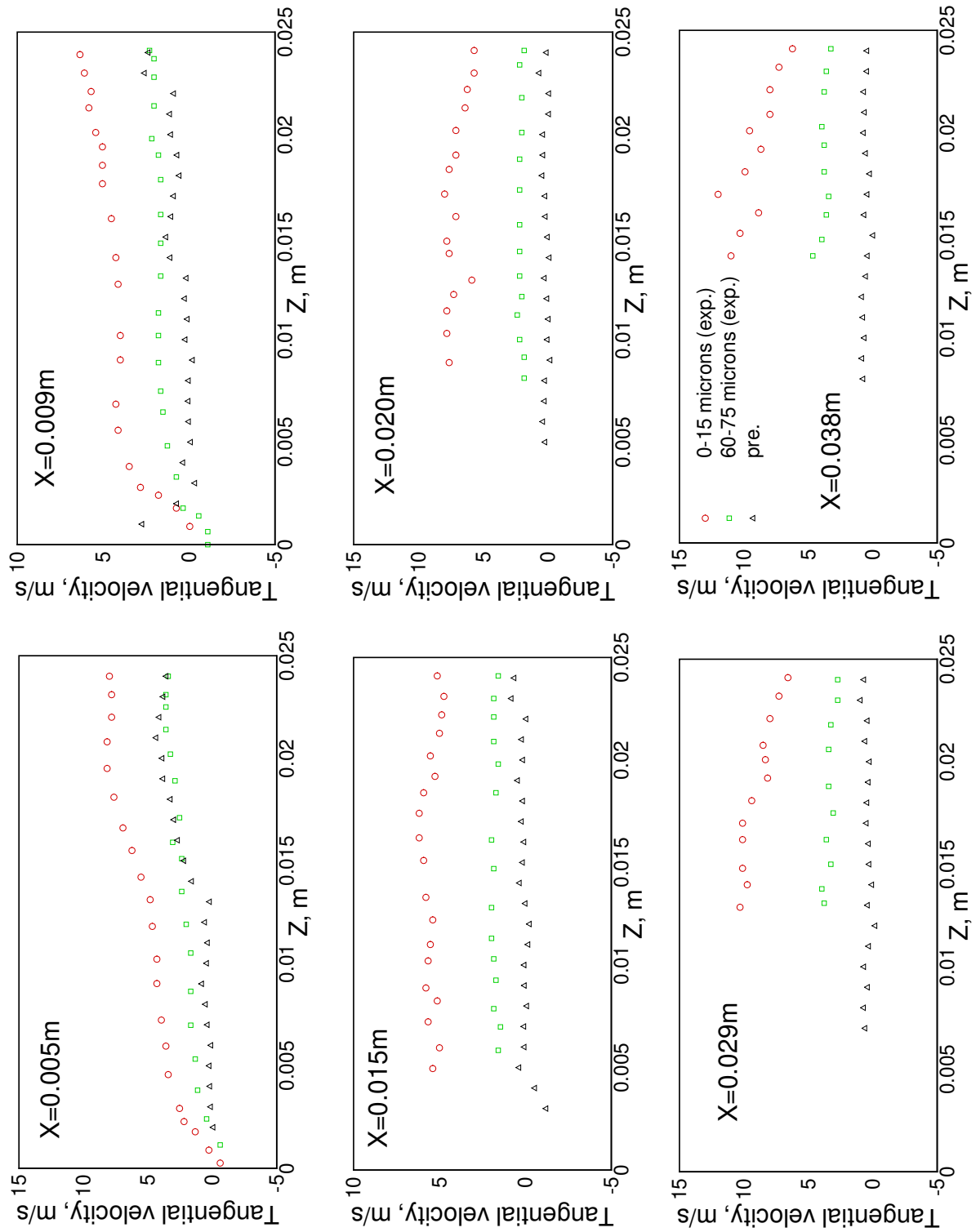Fig. 26 Spray mean radial velocity distributions.

Fig. 27 Spray mean tangential velocity distributions.

			Form Approved OMB No. 0704-0188

REPORT DOCUMENTATION PAGE

The public reporting burden for this collection of information is estimated to average 1 hour per response, including the time for reviewing instructions, searching existing data sources, gathering and maintaining the data needed, and completing and reviewing the collection of information. Send comments regarding this burden estimate or any other aspect of this collection of information, including suggestions for reducing this burden, to Department of Defense, Washington Headquarters Services, Directorate for Information Operations and Reports (0704-0188), 1215 Jefferson Davis Highway, Suite 1204, Arlington, VA 22202-4302. Respondents should be aware that notwithstanding any other provision of law, no person shall be subject to any penalty for failing to comply with a collection of information if it does not display a currently valid OMB control number.
PLEASE DO NOT RETURN YOUR FORM TO THE ABOVE ADDRESS.

1. REPORT DATE (DD-MM-YYYY) 01-03-2011	2. REPORT TYPE Technical Memorandum	3. DATES COVERED (From - To)

4. TITLE AND SUBTITLE Assessment of Some Atomization Models Used in Spray Calculations	5a. CONTRACT NUMBER NNC06BA07B
	5b. GRANT NUMBER
	5c. PROGRAM ELEMENT NUMBER

6. AUTHOR(S) Raju, M., S.; Bulzan, Dan	5d. PROJECT NUMBER
	5e. TASK NUMBER
	5f. WORK UNIT NUMBER WBS 984754.02.07.03.19.02

7. PERFORMING ORGANIZATION NAME(S) AND ADDRESS(ES) National Aeronautics and Space Administration John H. Glenn Research Center at Lewis Field Cleveland, Ohio 44135-3191	8. PERFORMING ORGANIZATION REPORT NUMBER E-17694

9. SPONSORING/MONITORING AGENCY NAME(S) AND ADDRESS(ES) National Aeronautics and Space Administration Washington, DC 20546-0001	10. SPONSORING/MONITOR'S ACRONYM(S) NASA
	11. SPONSORING/MONITORING REPORT NUMBER NASA/TM-2011-217029

12. DISTRIBUTION/AVAILABILITY STATEMENT
Unclassified-Unlimited
Subject Categories: 07, 20, 61, and 64
Available electronically at http://www.sti.nasa.gov
This publication is available from the NASA Center for AeroSpace Information, 443-757-5802

13. SUPPLEMENTARY NOTES

14. ABSTRACT
The paper presents the results from a validation study undertaken as a part of the NASA's fundamental aeronautics initiative on high altitude emissions in order to assess the accuracy of several atomization models used in both non-superheat and superheat spray calculations. As a part of this investigation we have undertaken the validation based on four different cases to investigate the spray characteristics of (1) a flashing jet generated by the sudden release of pressurized R134A from cylindrical nozzle, (2) a liquid jet atomizing in a subsonic cross flow, (3) a Parker-Hannifin pressure swirl atomizer, and (4) a single-element Lean Direct Injector (LDI) combustor experiment. These cases were chosen because of their importance in some aerospace applications. The validation is based on some 3D and axisymmetric calculations involving both reacting and non-reacting sprays. In general, the predicted results provide reasonable agreement for both mean droplet sizes (D32) and average droplet velocities but mostly underestimate the droplets sizes in the inner radial region of a cylindrical jet.

15. SUBJECT TERMS
Spray combustion; CFD modeling; Atomization; Turbulent combustion; Superheat spray

16. SECURITY CLASSIFICATION OF:			17. LIMITATION OF ABSTRACT	18. NUMBER OF PAGES	19a. NAME OF RESPONSIBLE PERSON STI Help Desk (email:help@sti.nasa.gov)
a. REPORT U	b. ABSTRACT U	c. THIS PAGE U	UU	42	19b. TELEPHONE NUMBER (include area code) 443-757-5802

Standard Form 298 (Rev. 8-98)
Prescribed by ANSI Std. Z39-18